electronics

MDPI

Article

Hydro–Wind–PV–Integrated Operation Optimization and Ultra-Short-Term HESS Configuration

Jinhua Zhang [1], Haizheng Wang [2], Chuanxi Fan [1,*], Jiahao Hu [1] and Xinyue Zhang [1]

[1] School of Electrical Engineering, North China University of Water Resources and Electric Power, Zhengzhou 450045, China; zhangjh@ncwu.edu.cn (J.Z.); hjh15138568829@gmail.com (J.H.); x20231050519@stu.ncwu.edu.cn (X.Z.)
[2] China Renewable Energy Engineering Institute, Beijing 100120, China; whz@creei.cn
* Correspondence: z202210050659@stu.ncwu.edu.cn

Abstract: In order to address the challenges associated with optimizing multi-timescale operations and allocating ultra-short-term energy storage for HWP integration, this study takes into account both the economic and reliability aspects of the HWP integration base. It proposes a model for optimizing operations and allocating energy storage capacity, achieving optimization across long-term, short-term, and ultra-short-term operations for an MECB. Initially, operation optimization is implemented for an entire group of terraced hydropower plants by regulating them with annual regulating capabilities on a long-term timescale. The objectives are to maximize the daily average minimum output and annual power generation. Subsequently, short-term operation optimization focuses on maximizing HWP power feed-in, minimizing new energy power curtailment, and reducing residual load standard deviation while ensuring the guaranteed output optimization results for the long term. Finally, to mitigate ultra-short-term fluctuations in new energy, a HESS with specified capacity and power is configured with the goal of minimizing comprehensive costs. Additionally, to address the challenge of smoothing negative fluctuations, which is hindered by charging and discharging efficiency limitations, a variable baseline is introduced, deviating from the conventional 0 MW baseline. A simulation study based on data from the hydro–wind–PV hybrid project in the Beipanjiang River Basin, China, demonstrates the following: (1) after long-term system optimization, the total power generation capacity of the system increases by 9.68%, while the peak-to-valley difference in output is significantly reduced; (2) short-term system optimization significantly reduces both the average variance in residual loads and the amount of power curtailed over five representative days; (3) the system incorporates 398.62 MWh of lithium-ion battery storage with a power of 412.47 MW and 51.09 MWh of supercapacitor storage with a power of 223.32 MW, which, together, completely smooth out the ultra-short-term fluctuations in new energy output.

Keywords: multi-energy complementarity; multiple timescales; operation optimization; storage allocation; CPO; TTAO

check for updates

Citation: Zhang, J.; Wang, H.; Fan, C.; Hu, J.; Zhang, X. Hydro–Wind–PV–Integrated Operation Optimization and Ultra-Short-Term HESS Configuration. *Electronics* **2024**, *13*, 4778. https://doi.org/10.3390/electronics13234778

Academic Editor: Jianguo Zhu

Received: 4 November 2024
Revised: 26 November 2024
Accepted: 30 November 2024
Published: 3 December 2024

Copyright: © 2024 by the authors. Licensee MDPI, Basel, Switzerland. This article is an open access article distributed under the terms and conditions of the Creative Commons Attribution (CC BY) license (https://creativecommons.org/licenses/by/4.0/).

1. Introduction

To address the challenges posed by energy consumption amidst economic globalization and global climate change, there is a need to transition energy production and utilization from fossil fuels like coal and oil to renewable sources such as wind and solar energy [1–3]. Wind and PV power exhibit strong stochasticity, volatility, and intermittency. Their large-scale integration into the power grid exacerbates the challenges of achieving spatial and temporal balance within the power system, thereby introducing new issues related to energy consumption [4,5]. To enhance the integration of PV and wind power into modern power grids, hydropower is frequently combined with PV and wind due to its high flexibility. This complementarity among various power sources facilitates the development of HRESs [6]. Integrated operations with water, wind, and solar power enable the use of

hydropower's regulatory capabilities to mitigate fluctuations in wind and photovoltaic outputs. This supports the grid's consumption of these energy forms while the different output characteristics of wind, photovoltaics, and hydropower are effectively regulated to ensure a stable electricity supply [7]. Consequently, constructing an integrated HWP system and conducting synergistic optimization research are of considerable significance [8]. To address the impact on grids due to large-scale wind and solar power consumption in river basins within the context of a new power system, this study redefines hydropower's role, evolving it from merely a "power supplier" to both a "power supplier and energy storage regulator". On a long-term to ultra-short-term timescale, this paper proposes an HWP-integrated operation optimization and energy storage capacity allocation model. This model optimizes HWP integration across long-term, short-term, and ultra-short-term operations amid the integration of new energy sources into the hydropower transmission channel and advances research into ultra-short-term energy storage capacity allocation [9,10].

Ma, C., et al. [11] presented a research framework aimed at determining optimal capacity allocation and short-term coordinated operation rules by considering the operational requirements of UHV transmission and hydropower plants. This framework includes a joint wind and PV scenario analysis technique, taking into account uncertainty and correlation, as well as a two-phase adaptive complementary operation strategy. Apostolopoulou, D., et al. [12] introduced an optimal scheduling scheme for a cascaded hydro–photovoltaic hybrid power generation system, focusing on maximizing the headwater level of each dam and minimizing spillage effects. Tan, Q., et al. [13] examined the risks and benefits associated with operating a large-scale HWP system while accounting for forecast uncertainty. Liu, W., et al. [14] explored a multi-objective optimization model for HWP systems, considering both power generation stability and river ecosystem impacts, utilizing an adaptive evolutionary algorithm. Additionally, they introduced a stochastic multi-criteria decision-making model to address decision-making uncertainty. He, Y., et al. [15] explored the optimal capacity allocation for an HWP hybrid system and developed a model using a chaotic local search of DE to minimize energy abandonment and maximize transmission corridor utilization. Ren, Y., et al. [16] proposed a mathematical model encompassing three operating scenarios that consider output characteristics and uncertainties, leveraging the flexibility of hydro, wind, and PV to ensure smooth power output from the water–wind–solar system. Ming, B., et al. [17] developed a three-layer nested framework to solve the problem of optimally scheduling daily power generation for a large-scale hybrid hydro–PV plant. Zhang, Y., et al. [18] calculated the optimal capacity ratio for the HWP system by minimizing cumulative fluctuations, based on complementary guarantees and cumulative time ratios. Lu, L., et al. [19] developed a coordinated operation model for an HWP hybrid energy system, taking into account wind and PV power uncertainty, ecological flow demand, and grid requirements based on mixed integer linear programming. Zhang, Y., et al. [20] proposed a short-term optimal operation model for a terraced hydro–PV hybrid energy system and a synchronized peaking strategy for terraced hydroelectric power plants based on fluctuation coefficients. Tan, Q., et al. [21] introduced a comprehensive flexibility index to quantify the regulation capacity of hydropower and EES, providing a foundation for the coordinated scheduling of hydropower–EES hybrid systems. A three-layer nested model—comprising "day-ahead", "intraday", and "real-time" layers—was developed to coordinate the joint dispatch of hydropower units and EESs at short-term and real-time levels. Gao, X., et al. [22] proposed a capacity allocation optimization method for a HESS using CEEMDAN to enhance the reliability and economic efficiency of microgrid operations. Zhang, J., et al. [23] introduced a method for the rational allocation of energy storage capacity within distribution networks characterized by significant PV penetration. Xie, D., et al. [24] introduced an FTC technique utilizing online vector computation and a constraint mechanism to address the operation of a single-phase CHBMC under multiple OC switch failures. This method optimizes DC voltage balance, minimizes the THD of grid-side currents, and ensures uniform power distribution between faulty and healthy batteries.

This paper proposes an operation optimization and energy storage capacity allocation model for HWP integration based on the regulating capacity of terraced hydropower plants

across long-term and short-term timescales, considering the economy and reliability of the integration base. First, operation optimization for the entire group of terraced hydropower stations is conducted by regulating those with annual regulating capabilities over a long-term timescale, aiming for maximum daily average output and annual power generation. Then, short-term operation optimization of the hydropower stations is performed with the goals of maximizing HWP power feed-in, minimizing new energy power curtailment, and reducing residual load variance based on the long-term guaranteed output optimization results [25]. To suppress ultra-short-term fluctuations in wind and PV power, the specific capacity and power of the supercapacitor energy storage are considered. Ultimately, optimal scheduling across long-, short-, and ultra-short-term periods for multi-energy complementary bases involving hydro, wind, PV, and ES is achieved.

The main contributions made by this study are listed below:

- This paper develops a long-term, short-term, and ultra-short-term optimal allocation system for integrated hydro, wind, PV, and energy storage. The system considers hydropower regulation capacity, new energy curtailment, guaranteed output, and the comprehensive cost of the energy storage system.
- Operation optimization of the entire HWP integration base is conducted on a long-term timescale by adjusting the daily average flow rate of hydropower plants with annual regulation capacity. The objectives are to maximize the daily minimum average output and annual power generation. The optimization model is solved using TTAO to achieve long-term optimal scheduling.
- Building on the long-term optimization results, short-term scheduling is performed to regulate the hourly output of each hydropower station. The objectives here include maximizing the integration of HWP power, minimizing new energy curtailment, and reducing the standard deviation of the residual load, thereby achieving short-term optimal dispatching.
- For ultra-short-term fluctuations, battery storage and supercapacitors are configured based on the installed capacities of wind and photovoltaic systems, as well as the annual output on a 5-min timescale. The goal is to minimize the integrated cost of the HESS while completely smoothing ultra-short-term fluctuations in new energy sources. CPO is also used to optimize the parameters of ICEEMDAN during the power decomposition process, ensuring better decomposition performance. To address the challenge of smoothing negative fluctuations around the zero baseline, the model introduces a variable baseline. This approach improves fluctuation smoothing performance and reduces costs by requiring a smaller HESS capacity.

The main contents of this paper are organized as follows: Section 2 presents the long-term optimization model aimed at achieving both maximum guaranteed output and maximum power generation for HWP integration. Section 3 details the short-term optimization model, which aims to maximize net power from HWP integration, minimize the curtailment of new energy, and reduce fluctuations in residual load power. Section 4 introduces the ultra-short-term energy storage optimization model, which employs CPO-ICEEMDAN to reconstruct the low-frequency components of raw new energy power. Section 5 verifies the feasibility of the HWP integration multi-timescale cooperative optimization model through example calculations and analyses. Section 6 provides a comprehensive summary of the paper and discusses the results obtained.

2. Long-Term Optimization Model for Hydro–Wind–PV Integration

When hydropower, wind power, and photovoltaic systems operate jointly over an extended period, they primarily depend on the reservoir's regulating capacity to balance excess and scarcity in the base hydropower and to augment output during dry periods. For hydropower stations with long-term regulation capacity, or for terraced hydropower station groups that include long-term regulation stations, a well-designed long-term scheduling plan directly influences the scheduling and operational efficiency of the entire system over one or multiple years. Especially with the large-scale integration of new energy,

hydropower assumes a central role in the HWP hybrid power system. Therefore, in formulating a long-term plan for hydropower, it is crucial to fully explore the potential for compensation and the peak shifting of terraced hydropower stations in each period and to consider the benefits of hydropower stations' power and capacity. This ensures the safe and efficient operation of the power system with a high proportion of new energy integrated into the grid.

2.1. Long-Term Optimization Model Objective Function

In line with the purpose of constructing an MECB, the objectives of the long-term optimal dispatch are set as maximizing the guaranteed output and the annual power generation of the HWP integration base.

(1) Maximum guaranteed output

The output during the minimum output period within the calculation cycle impacts the guaranteed output of the MECB. Therefore, the minimum output should be maximized. To achieve this, a maximized minimum output target is defined, expressed as

$$f_1 = max\left\{\min\left[\sum_{j\in\{h,w,s\}} N_t^j\right]\right\} \tag{1}$$

In the formula, f_1 is the optimization target of the water and wind power system output; n is the total number of power stations in category $j \in \{h,w,s\}$; $j \in \{h,w,s\}$ represents the hydroelectric power station, the wind power station, and the photovoltaic power station, respectively; N_{jmt} represents the power generation output of power stations in category j in time period t, MW.

(2) Maximum annual electricity generation

The annual power generation of the HWP system reflects the economic benefits of the MECB. Therefore, the objective of maximizing the total HWP generation over the calculation cycle (one year) is expressed as

$$f_2 = Max\left\{\sum_{t=1}^{T}\sum_{j\in\{h,w,s\}}\left[N_t^j \times \Delta t\right]\right\} \tag{2}$$

In the formula, f_2 is the annual power generation optimization target of the water–wind–scenery system and the total power generation of the hydro–wind–PV complementary system in the whole period; T is the whole optimization period; and the meanings of the rest of the parameters are the same as above.

(3) Linear weighting

Based on the linear weighted sum method, the objective functions f_1 and f_2 are normalized with the following equations:

$$\begin{cases} \max F = \lambda_{k,1}\left(\frac{f_1 - f_1^{\min}}{f_1^{\max} - f_1^{\min}}\right) + \lambda_{k,2}\left(\frac{f_2 - f_2^{\min}}{f_2^{\max} - f_2^{\min}}\right) \\ \lambda_{k,1} + \lambda_{k,2} = 1 \end{cases} \tag{3}$$

In the formula, F is the multi-objective optimization function of the vehicle; $f_1^{\max}$ and $f_2^{\max}$ are the maximum values of the single-objective functions f_1 and f_1, respectively; and $\lambda_{k,1}$ and $\lambda_{k,2}$ are the optimization weights of the single-objective functions, f_1 and f_1, respectively.

2.2. Long-Term Optimization Model Restrictive Condition

(1) Reservoir storage constraint

$$C_{\min}^{m} \le C_{t}^{m} \le C_{\max}^{m} \tag{4}$$

In the formula, $C_{\min}^{m}$ and $C_{\max}^{m}$ are the upper and lower limits of the reservoir capacity of the hydroelectric power plant.

(2) Reservoir discharge flow constraint

$$Q_{t,\min}^{O,m} \le Q_{t}^{O,m} \le Q_{t,\max}^{O,m} \tag{5}$$

In the formula, $Q_{t,\min}^{O,m}$ and $Q_{t,\max}^{O,m}$ are the upper and lower limits of the discharge flow of the hydropower plant, respectively.

(3) Hydroelectric power plant generation flow constraint

$$Q_{t,\min}^{E,m} \le Q_{t}^{E,m} \le Q_{t,\max}^{E,m} \tag{6}$$

In the formula, $Q_{t,\min}^{E,m}$ and $Q_{t,\max}^{E,m}$ are the upper and lower limits of the generation flow moment t of the m hydroelectric power plant, respectively.

(4) Hydraulic links between terraced hydroelectric plants

$$Q_{t}^{I,m} = Q_{t}^{O,m-1} + Q_{t}^{Ir,m} \tag{7}$$

In the formula, $Q_{t}^{I,m}$ is the reservoir flow of the hydropower station; $Q_{t}^{Ir,m}$ is the interval runoff of the hydropower station.

(5) Terraced hydropower plant output constraint

$$N_{t,\min}^{H,m} \le N_{t}^{H,m} \le N_{t,\max}^{H,m} \tag{8}$$

In the formula, $N_{t,\min}^{H,m}$ and $N_{t,\max}^{H,m}$ are the upper and lower limits of the output of the hydropower plant, respectively.

(6) Electricity transmission channel constraint

$$P_{t,\min}^{m} \le P_{t}^{m} \le P_{t,\max}^{m} \tag{9}$$

In the formula, $P_{t,\min}^{m}$ and $P_{t,\max}^{m}$ are the upper and lower limits of the power transmission channel of the hydropower plant.

(7) Reservoir capacity–water level relationship

$$C_{m,n} = f_{m}^{zv}(Z_{m,n}) \tag{10}$$

In the formula, $f_{m}^{zv}(g)$ is the nonlinear relationship function between the upstream water level, $Z_{m,n}$, and the reservoir capacity of hydropower station m; $Z_{m,n}$ is the upstream reservoir capacity level (m) of the hydropower station.

(8) Tailwater level–discharge flow rate relationship

$$Z_{m,n}^{d} = f_{m}^{down}(Q_{n}^{o,m}) \tag{11}$$

In the formula, $f_{m}^{down}(Q_{m,n})$ is the nonlinear relationship function between the discharged flow rate and the tailwater level of hydropower plant m; $Z_{m,n}^{d}$ is the tailwater level; and $Q_{n}^{o,m}$ is the discharged flow rate.

In summary, an HWP long-term complementary optimization strategy is crucial for ensuring high power supply quality and enhancing energy utilization efficiency. The process of HWP long-term complementary optimization is depicted in Figure 1.

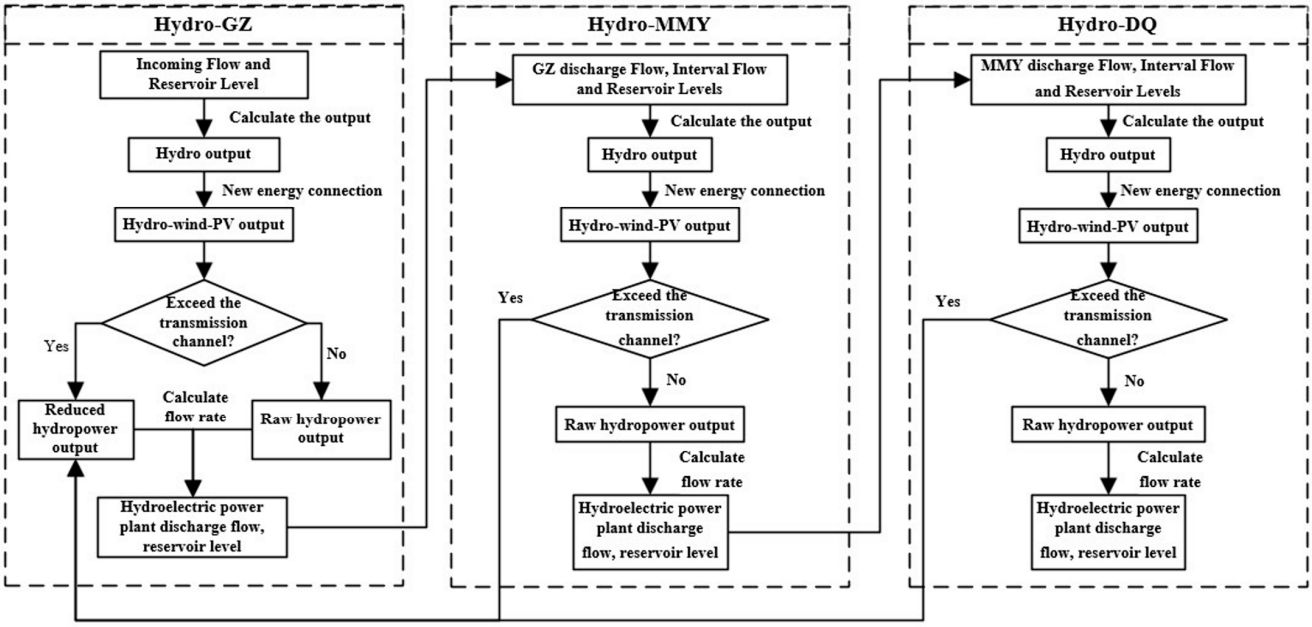


Figure 1. Flowchart of long-term optimization.

2.3. Solution Method

In this paper, the long-term optimization model is solved using the Triangulation Topology Aggregation Optimizer (TTAO), a novel, mathematically inspired metaheuristic algorithm proposed by S. Zhao et al. in 2024 for solving continuous optimization problems and engineering applications [26]. The algorithm leverages the principles of similar triangle topology from mathematics to strike a balance between exploration and exploitation through two strategies: generic aggregation and local aggregation. Compared to algorithms such as PSO, DBO [27], and RIME [28], TTAO employs the geometrical properties of triangular topology to dynamically adjust populations, enhancing the diversity of search directions and significantly improving global search capabilities. At the same time, its use of aggregation relationships within the topology refines local searches, preventing the sparsity of global transitions from undermining local search performance.

3. Short-Term Optimization Model for Hydro–Wind–PV Integration

The short-term complementary operation of hydro, wind, and photovoltaic power primarily involves using the regulatory capabilities of hydroelectric power stations to initially stabilize wind and photovoltaic power outputs. Subsequently, hydropower output is adjusted according to system load demands and transmission capacity, aiming to maximize wind and solar power consumption without increasing water spillage from hydropower. Specifically, when wind and solar power outputs are high, hydropower output is reduced through methods such as water storage. Conversely, when wind and solar outputs are low, hydropower output is increased, effectively storing new energy in reservoirs for temporal transformation and redistribution, thus meeting power system demands collectively.

Short-term operation optimization typically relies on the water and power control conditions established by long-term optimal dispatch to guide the real-time management of power stations. In contrast to long-term operations, the short-term timescale is brief, and the stochastic and intermittent nature of wind and solar energy is pronounced. Consequently, the objectives are to maximize HWP power integration, minimize new energy curtailment, and reduce fluctuations in residual load power, thereby ensuring a balance between economic efficiency and power quality.

This paper presents a short-term optimization model for integrated HWP energy, primarily grounded on the daily average output and the initial and final reservoir capacities

derived from long-term optimization. It seeks to optimize the hydropower plant's output within a 24 h period to achieve short-term complementary integration.

3.1. Short-Term Optimization Model Objective Function

In alignment with the construction goals of the MECB, the short-term optimization scheduling objectives include minimizing the standard deviation of the residual load in the HWP integration, maximizing the HWP grid-connected electricity, and minimizing new energy power curtailment. The specific expressions for each optimization objective are detailed as follows:

$$\min P = \min(\lambda_1 P_{STD} - \lambda_2 N + \lambda_3 P_{EWR}) \tag{12}$$

In the formula, P_{STD}, N, and P_{EWR} are the standard deviation of the remaining load, the hydro–wind–photovoltaic grid-connected electricity, and the target of new energy power abandonment, respectively; λ_1, λ_2, and λ_3 are the coefficients of the three targets, respectively.

(1) Minimum standard deviation of residual load

The residual load standard deviation measures the average of the squared error between power output and load demand, representing the overall degree of residual load fluctuation. A larger standard deviation indicates a greater deviation between the output and load. The mathematical formula is expressed as:

$$\min P_{STD} = std[N_{load} - N_{grid}] \tag{13}$$

In the formula, N_{load} is the load demand power in the region; N_{grid} is the sum of wind, photovoltaic, and hydro online power.

(2) Maximum integrated HWP grid-connected electricity

The grid-connected electricity of the HWP integration system reflects its economic performance. More grid-connected electricity indicates a better system economy. The mathematical formula is expressed as

$$\max N = \sum_{t=1}^{n} [N_{WT,grid}(t) + N_{PV,grid}(t) + N_{HY,drid}(t)] \times \Delta t \tag{14}$$

In the formula, $N_{WT,grid}(t)$, $N_{PV,grid}(t)$, and $N_{HY,grid}(i)$ are the wind power, photovoltaic power, and hydropower delivered to the grid.

(3) Minimum new energy abandonment

The size of new energy power abandonment reflects the economic efficiency and complementarity of integrating new energy sources into a hydropower station's power transmission channel. Smaller new energy power abandonment indicates a better economy and the complementarity of the HWP integration system. The mathematical formula is expressed as

$$\min P_{EWR} = \sum_{t=1}^{T} \left[N_{PV}(t) + N_{WT}(t) - N_{NE.grid}(t) \right] \times \Delta t \tag{15}$$

In the formula, P_{EWR} is the new energy electricity abandonment in the optimization period; $N_{WT}(t)$ and $N_{PV}(t)$ are wind power and photovoltaic power; and $N_{NE.grid}(t)$ is the new energy power delivered to the grid.

3.2. Short-Term Optimization Model Restrictive Condition

(1) Reservoir storage constraint

$$\begin{array}{l} C_{\min}^{m} \le C_{t}^{m} \le C_{\max}^{m} \\ C_{i,m} = C_{m}^{start} \\ C_{e,m} = C_{m}^{end} \end{array} \tag{16}$$

In the formula, $C_{\min}^{m}$ and $C_{\max}^{m}$ are the upper and lower limits of the reservoir capacity of the hydropower plant, respectively; C_{m}^{start} and C_{m}^{end} are the starting and final reservoir capacity of the hydropower plant for the short-term scheduling period.

Constraints (2)–(8) are the same as those in Section 2.2.

An HWP short-term complementary optimization strategy is crucial for meeting grid load demands and minimizing resource waste. The process is depicted in Figure 2.

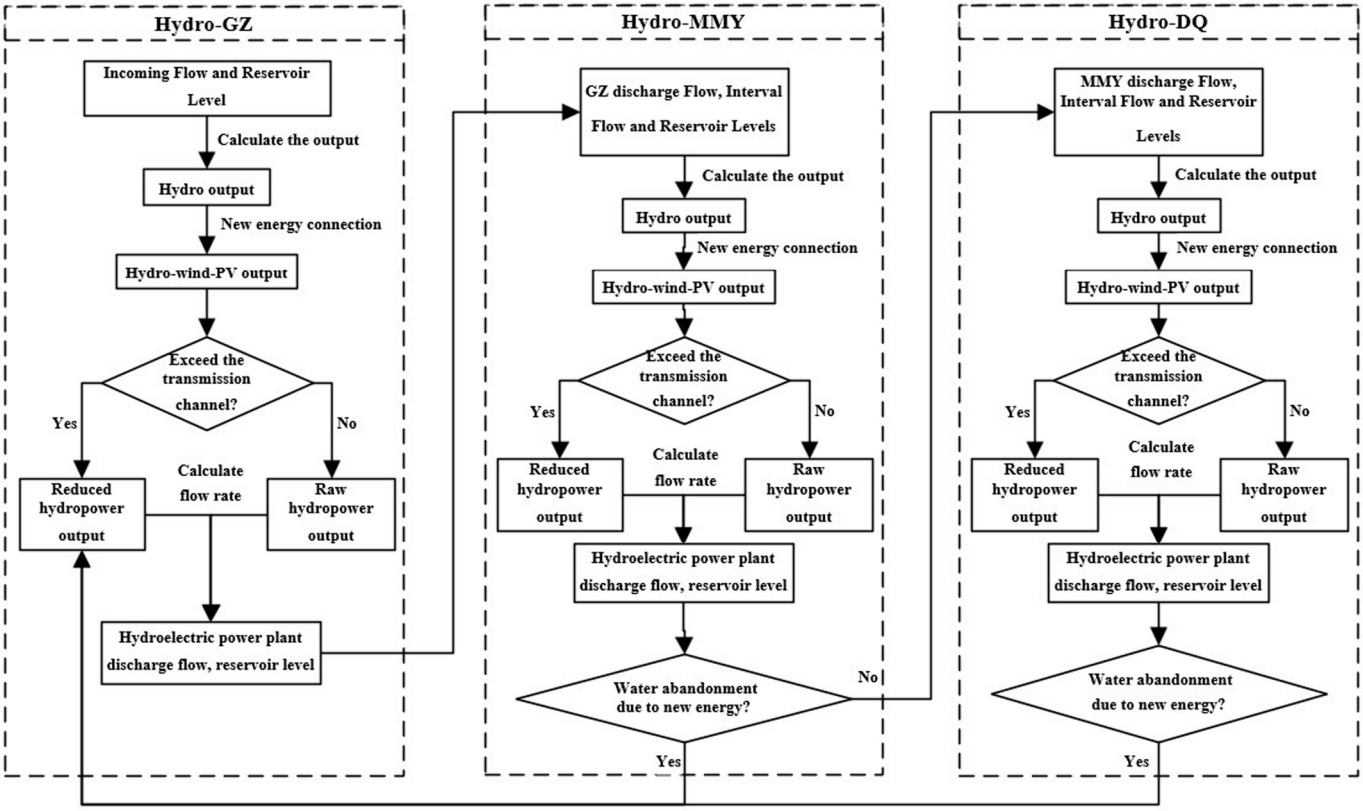


Figure 2. Flowchart of short-term optimization.

4. Ultra-Short-Term Energy Storage Optimal Allocation Model

While the long-term and short-term complementary operation optimization of hydro–wind–PV systems can be managed through the regulating capabilities of hydropower plants, significant fluctuations in wind and solar power at ultra-short-term timescales pose challenges. The inherent characteristics of hydropower units prevent them from effectively responding to and regulating these ultra-short-term fluctuations. A HESS, consisting of battery and capacitor energy storage, is well suited for scenarios requiring short-term high power and multiple cyclic discharges due to its high power and long life-cycle characteristics. Therefore, this paper proposes configuring a specific lithium-ion battery and supercapacitor energy storage capacity to smooth out ultra-short-term fluctuations in new energy output. The ultra-short-term energy storage allocation model employs K-means clustering to categorize annual new energy output into six clusters, constructing typical periods for ultra-short-term energy storage allocation based on the median of each cluster. CPO-ICEEMDAN is used to process the raw signals from new energy sources. The signal decomposition results are categorized into direct grid-connected components and energy storage smoothing components by selecting suitable 10 min fluctuation limits. Finally, the HESS capacity is configured to ensure cost minimization.

4.1. New Energy Power Allocation Based on CPO-ICEEMDAN

ICEEMDAN is utilized to process the original new energy raw signal to obtain each order for Intrinsic Mode Functions (IMFs). Processing each IMF component individually

can create an unnecessary workload, so a suitable fluctuation threshold for grid connection is chosen. The decomposed signal is then reconstructed into low-frequency and high-frequency components. Low-frequency components that meet grid connection requirements are directly connected to the grid, while high-frequency components that do not meet these requirements are managed by the HESS.

The decomposition effect of the ICEEMDAN method depends on two key parameters: the white noise amplitude weight (Nstd) and the noise rates (NRs). Optimizing these parameters can reduce the modal aliasing phenomenon, thereby achieving better power decomposition performance [29]. To this end, CPO is utilized to optimize the parameters of ICEEMDAN. The fitness function is based on envelope entropy, where a smaller fitness value indicates a superior decomposition effect. Through iterative optimization and parameter updates, the optimal combination of Nstd and NR is determined.

The Crested Porcupine Optimizer (CPO) is a metaheuristic algorithm proposed by M. Abdel-Basset et al. in 2024, inspired by the defensive behavior of the crested porcupine [30]. CPO employs four distinct protection mechanisms: sight, sound, odor, and physical attacks. The first two strategies (sight and sound) represent the algorithm's exploratory capabilities, while the latter two (odor and physical attacks) emphasize exploitative behavior.

Compared with methods such as PSO, WOA [31], NGO [32], and RIME, CPO dynamically adjusts its behavioral patterns during the iterative process, achieving a more effective balance between exploration and exploitation. By mimicking the porcupine's pursuit and avoidance strategies, CPO can rapidly converge toward the optimal solution. Additionally, the inclusion of random perturbations and behavioral adaptations enhances population diversity, improving the ability to escape local optima. In solving multimodal optimization problems, which are characterized by multiple local optima, CPO demonstrates superior performance by effectively identifying and escaping from local extremes. Its enhanced global optimization ability makes it more robust and effective for complex optimization problems.

The high-frequency reconstruction generates high-frequency components for each order based on the top-down superposition of the CPO-ICEEMDAN decomposition results. The specific reconstruction method is detailed in Equation (17).

$$\begin{cases} f2c(1) = IMF1 \\ f2c(2) = IMF1 + IMF2 \\ \vdots \\ f2c(p+1) = IMF1 + IMF2 + \ldots + IMFp + res \end{cases} \tag{17}$$

The low-frequency reconstruction creates low-frequency components for each order through the bottom-up superposition of the CPO-ICEEMDAN decomposition results, as outlined in Equation (18).

$$\begin{cases} c2f(1) = res \\ c2f(2) = res + IMFp \\ \vdots \\ c2f(p+1) = res + IMFp + \ldots + IMF1 \end{cases} \tag{18}$$

Following signal decomposition and reconstruction, power allocation is achieved through the NE power allocation strategy. A flowchart detailing the CPO-ICEEMDAN-based power allocation strategy is shown in Figure 3.

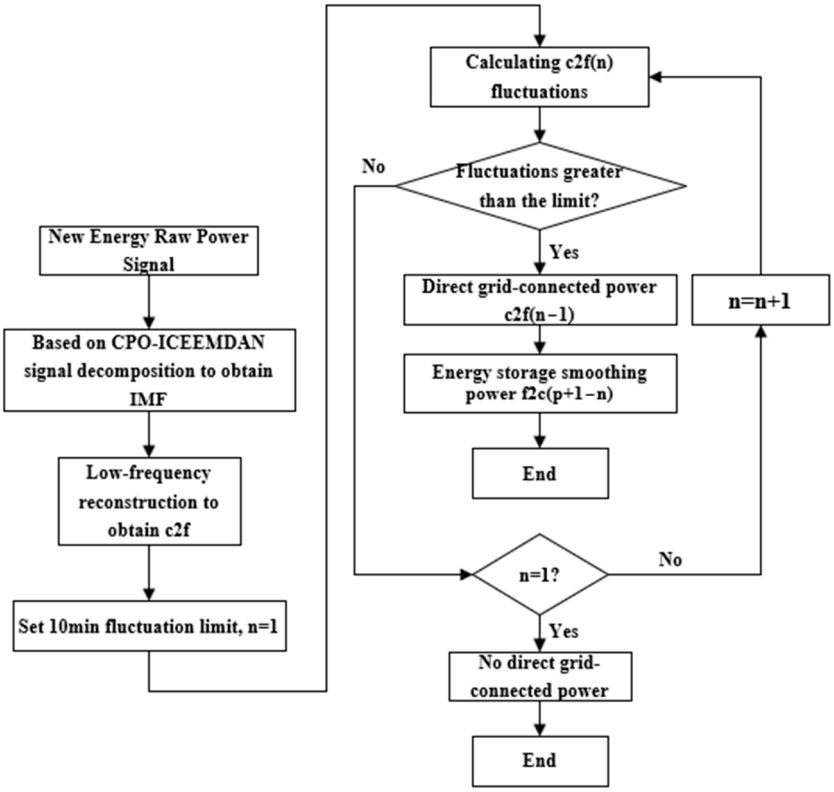


Figure 3. Flowchart showing CPO-ICEEMDAN-based power allocation strategy.

4.2. Ultra-Short-Term Energy Storage Optimal Allocation Model Objective Function

Section 4.1 derives the power assignment, P_{ES}, for the HESS using the CPO-ICEEMDAN power allocation method. Utilizing P_{ES} and considering the operational characteristics of the HESS, a capacity and power allocation model is established to smooth the fluctuations of the new energy output.

The integrated cost of the energy storage system includes the supercapacitor energy storage cost, the lithium-ion battery energy storage cost, the operation and maintenance costs, and the residual fluctuation penalty cost. The objective function is provided in Equation (19):

$$\min C = C_{SC} + C_{Li} + C_{NE}^{flu} \tag{19}$$

In the formula, C is the annual comprehensive cost; C_{SC} is the cost of supercapacitor energy storage; C_{Li} is the cost of lithium-ion battery energy storage; and C_{NE}^{dit} is the cost of compensation for new energy power fluctuation opportunities.

(1) Investment cost and operation and maintenance costs of supercapacitor

The system is connected to a large power grid, and if the power generation cannot meet the system load, it is necessary to purchase power from the grid, incurring a cost:

$$C_{CS} = C_{CS}^{o} + C_{CS}^{m} \tag{20}$$

$$C_{CS}^{o} = (\lambda_{CSP} P_{CS} + \lambda_{CSE} E_{CS}) \frac{r(1+r)^{y}}{(1+r)^{y} - 1} \tag{21}$$

$$C_{CS}^{m} = \alpha_{Li} C_{CS}^{o} \tag{22}$$

In the formula, C_{CS} is the investment cost of the supercapacitor; C_{CS}^{o} is the primary installation cost of the supercapacitor; C_{CS}^{m} is the operation and maintenance costs of the supercapacitor; λ_{CSP} is the cost coefficient of the unit power of the supercapacitor; λ_{CSE} is the cost coefficient of the unit capacity of the supercapacitor; P_{CS} is the rated power of

the supercapacitor; E_{CS} is the rated capacity of the supercapacitor; r is the discount rate; y is the service life of the supercapacitor; and α_{Li} is the cost coefficient of the operation and maintenance of the supercapacitor.

(2) Investment cost and operation and maintenance costs of lithium-ion battery

$$C_{Li} = C_{Li}^{o} + C_{Li}^{m} \tag{23}$$

$$C_{Li}^{o} = (\lambda_{LiP} P_{Li} + \lambda_{LiE} E_{Li}) \frac{r(1+r)^{y}}{(1+r)^{y} - 1} \tag{24}$$

$$C_{Li}^{m} = \alpha_{Li} C_{Li}^{o} \tag{25}$$

In the formula, C_{Li} is the investment cost of battery storage; C_{Li}^{o} is the primary installation cost of battery storage; C_{Li}^{m} is the operation and maintenance costs of battery storage; λ_{LiP} is the cost coefficient of battery storage per unit of power; λ_{LiE} is the cost coefficient of battery storage per unit of capacity; P_{Li} is the rated power of battery storage; E_{Li} is the rated capacity of battery storage; r is the discount rate; y is the service life of battery storage; α_{Li} is the cost coefficient of the operation and maintenance of battery storage.

(3) Residual fluctuation penalty cost

The residual volatility penalty cost represents the magnitude of the residual volatility component after configuring the HESS. Increasing its multiplier enhances its weight in the integrated cost, leading to improved smoothing performance but also raising the overall integrated cost. The mathematical expressions are provided in Equations (26) and (27):

$$C_{NE}^{flu} = a \times \eta_{pun} \times N_{flu} \tag{26}$$

$$N_{flu} = \sum_{n=1}^{N_s} T_{Day,n} (P_{P_flu,n} - P_{N_flu,n}) \tag{27}$$

In the formula, a is the multiplier; η_{pun} is the penalty cost coefficient, 0.24 CNY/kWh; $T_{Day,n}$ is the frequency of a typical day; and $P_{P_flu,n}$ and $P_{N_flu,n}$ are the positive and negative undercompensated quantities, respectively.

4.3. Constraints

(1) Charge–discharge power constraint

$$\begin{cases} 0 \le P_{SC,ch} \le P_{SC,\max} \\ 0 \le P_{SC,dis} \le P_{SC,\max} \\ 0 \le P_{Li,ch} \le P_{Li,\max} \\ 0 \le P_{Li,dis} \le P_{Li,\max} \\ P_{SC,dis} * P_{SC,\max} = 0 \\ P_{Li,dis} * P_{Li,\max} = 0 \end{cases} \tag{28}$$

In the formula, $P_{SC,ch}$ and $P_{Li,ch}$ are the charging power of the supercapacitor and the lithium-ion battery, respectively; $P_{SC,dis}$ and $P_{Li,dis}$ are the discharging power of the supercapacitor and the lithium-ion battery, respectively.

(2) Power balance constraint

Due to the impact of the charging and discharging efficiency of the HESS, achieving 0 MW of fluctuation at every moment is challenging, particularly for the negative fluctuations in P_{ES}. To address this, a variable baseline, P_{set}, is introduced to adjust the fluctuating power to approximately P_{set} at each moment. The optimal value of P_{set} will be determined during the calculation process.

The energy storage power task, P_{ES}, is divided into two parts: positive fluctuation and negative fluctuation. Positive fluctuation occurs when $P_{ES} > P_{set}$, requiring HESS

charging to absorb the fluctuation. Conversely, negative fluctuation occurs when $P_{ES} < P_{set}$, necessitating HESS discharging to compensate for the fluctuation.

$$P_{ES,n} = P_{SC,ch,n} - P_{SC,dis,n} + P_{Li,ch,n} - P_{Li,dis,n} + P_{set} + \Delta P_{flu,n} \tag{29}$$

In the formula, $\Delta P_{flu,n}$ represents the residual fluctuation at moment n.

(3) SOC constraint

$$SOC_{SC}(t) = SOC_{SC}(t-1) + \frac{(P_{SC,ch}(t)\eta_{ch} + P_{SC,dis}(t)/\eta_{dis})\Delta t}{E_{SC}} \tag{30}$$

$$SOC_{Li}(t) = SOC_{Li}(t-1) + \frac{(P_{Li,ch}(t)\eta_{ch} + P_{Li,dis}(t)/\eta_{dis})\Delta t}{E_{Li}} \tag{31}$$

$$SOC_{\min} \leq SOC_n \leq SOC_{\max} \tag{32}$$

In the formula, SOC denotes the state of charge of the battery. η_{ch} and η_{dis} represent the charging and discharging efficiencies of the battery, respectively. $SOC_{\max}$ and $SOC_{\min}$ are the maximum and minimum values of SOC, respectively.

5. Calculus Analysis

5.1. Results of Long-Term Optimization for a Hydro–Wind–PV System

5.1.1. Basic Parameters of Long-Term Optimization

The data analyzed in the calculations of this paper come from the hydro–wind–PV integration base of the Beipanjiang (BPJ) River in Guizhou Province, China.

Based on the specific geographic location and year-round climatic conditions of the Beipanjiang River, the boundary conditions are determined in conjunction with studies on the structural configurations of existing hydropower plants. The total installed capacity of the four terraced power stations is 2663.5 MW. From upstream to downstream, the stations are SNP (185.5 MW), GZ (1040 MW), MMY (558 MW), and DQ (880 MW). The regulating reservoirs and their corresponding regulation types are as follows: SNP (0.428 billion m^3, daily regulation), GZ (2.037 billion m^3, incomplete multi-year regulation), MMY (0.307 billion m^3, daily regulation), and DQ (143.8 million m^3, daily regulation).

In this study, the three power stations with larger installed capacities—GZ, MMY, and DQ—are considered. The maximum generation flow rate is 845.8 m^3/s at GZ, 880.83 m^3/s at MMY, and 934.4 m^3/s at DQ.

To support the development of future integrated HWP bases, plans are set for 2030 to expand the transmission capacity of the GZ to 1935 MW. In its vicinity, two wind farms with a combined installed capacity of 1600 MW and nine PV power plants with a total installed capacity of 1400 MW will be constructed. The transmission capacity of the MMY will remain unchanged, but a PV power plant with an installed capacity of 300 MW is planned nearby. For the DQ, its transmission capacity will be expanded to 1350 MW, accompanied by the construction of two wind farms with a combined installed capacity of 950 MW and eight PV power plants with a total installed capacity of 1200 MW. The electricity generated by the wind and PV power plants will first be processed at booster stations, then integrated with nearby hydropower plants, and transmitted collectively to the power grid via shared transmission channels.

(1) The GZ hydropower plant possesses an incomplete multi-year regulation capability, while the MMY and DQ hydropower plants are equipped with daily regulation capabilities. Due to the relatively stable long-term water levels of the MMY and DQ reservoirs, their operations primarily depend on the regulating capacity of the GZ hydropower station. By adjusting the discharged flow rate of the GZ hydropower station, complementary operation optimization on a long-term timescale can be achieved. The basic information for the three hydropower plants is presented in Table 1.

Table 1. Basic information for terraced hydropower stations.

Hydro	Maximum Reservoir Capacity (10^8 m^3)	Minimum Reservoir Capacity (10^8 m^3)	Regulatory Capability	Installed Capacity (MW)
GZ	32.45	10.98	incomplete multi-year regulation	1040
MMY	1.722	1.058	daily regulation	558
DQ	9.55	7.386	daily regulation	880

(2) The power transmission channel of the hydropower stations and the installed capacity of new energy in the vicinity are shown in Table 2.

Table 2. Transmission channel for hydroelectric power plants and installed capacity of new energy in the vicinity.

Hydro	Channel Limit (MW)	Wind Power (MW)	Photovoltaic (MW)
GZ	1935	1600	1400
MMY	558	0	300
DQ	1350	950	1200

5.1.2. Results Analysis of Long-Term Optimization

In this study, two scenarios were constructed for comparative analysis to evaluate the effectiveness of the long-term optimization model:

(1) Scenario 1: Optimization of hydro–wind–PV system alone;
(2) Scenario 2: Integrated optimization of hydro–wind–PV system.

In this paper, PSO, DBO, RIME, and TTAO were employed to solve the long-term optimization model for the HWP system. Each algorithm was tested with a population size of 210 and 800 iterations. Each algorithm was executed 20 times, and the results were analyzed. Box plots for each algorithm were generated to evaluate the guaranteed output objective (Equation (1)) and the generation objective (Equation (2)), as shown in Figure 4.

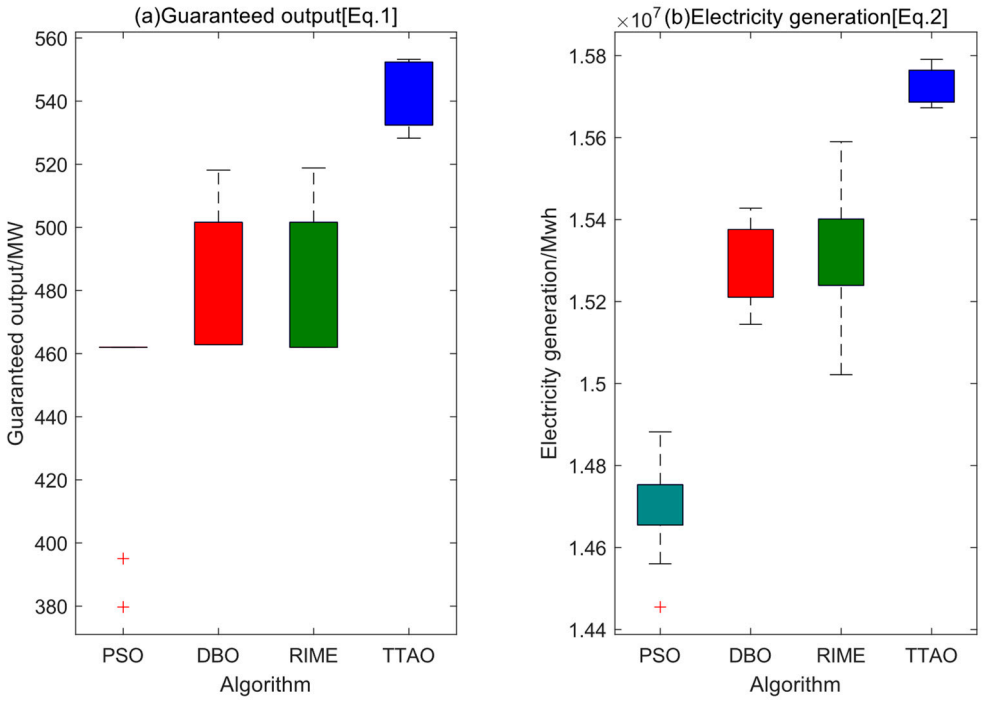


Figure 4. Optimization results box plots.

An analysis of the box plots reveals that the numerical values and stability of Equations (1) and (2), obtained using TTAO, are superior to those of the other algorithms. This indicates that TTAO offers distinct advantages in solving the long-term optimization model.

Out of the 20 results, a comparison of the optimal iteration curves for each algorithm with respect to the fitness function (Equation (3)) is presented in Figure 5. The figure shows that TTAO achieves better optimization results compared to the other algorithms.

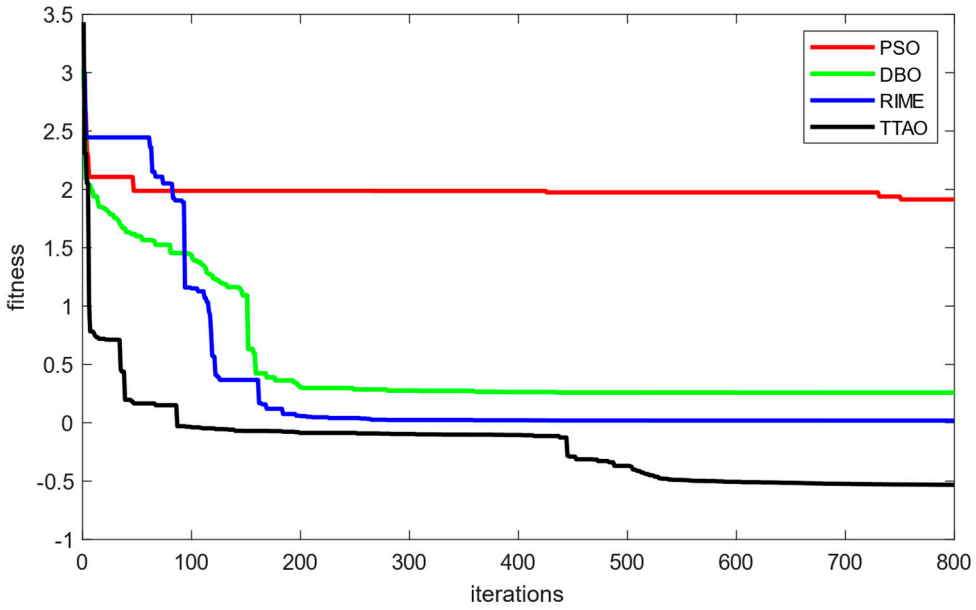


Figure 5. Comparison of different algorithms for solving Scenario 2.

TTAO was used to solve Scenarios 1 and 2. A daily average output comparison is shown in Figure 6, and the stacked monthly average output is depicted in Figure 7. Compared to Scenario 1, the monthly average output of Scenario 2 is significantly lower from June to August, while it is noticeably higher from October to February. Additionally, the output fluctuation on the long-term timescale is significantly reduced.

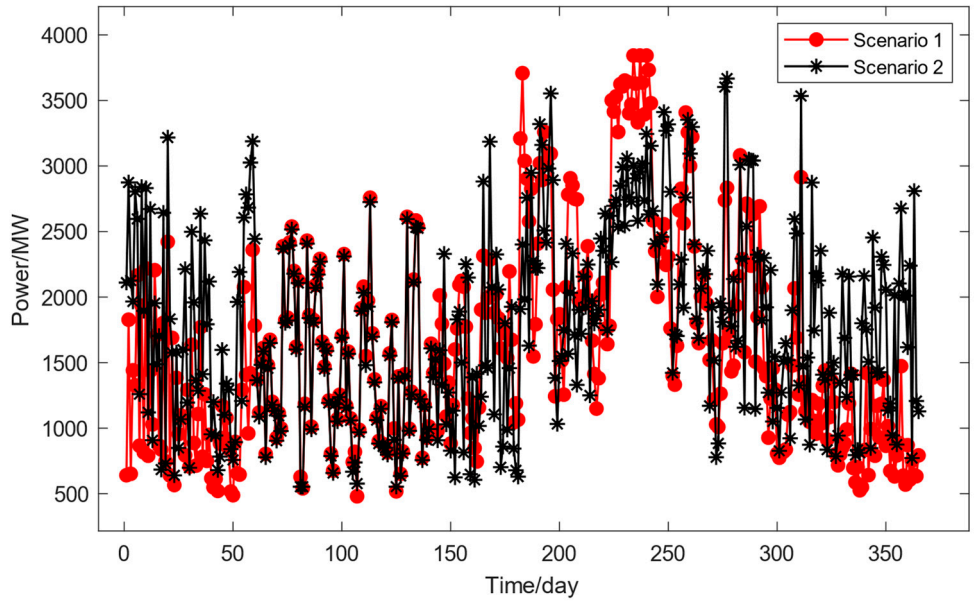


Figure 6. Average daily output of hydro–wind–PV system.

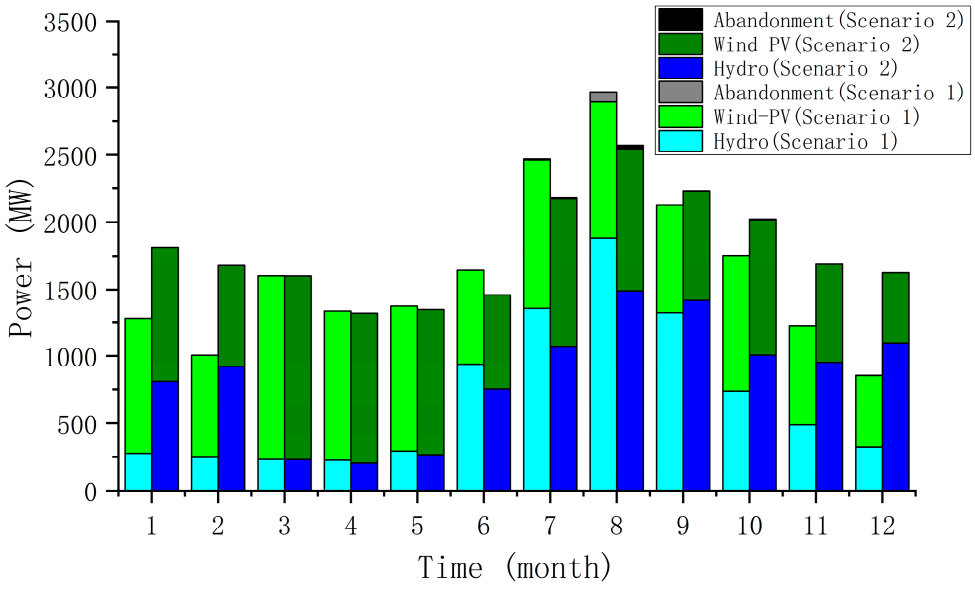


Figure 7. Average monthly output of hydro–wind–PV.

A comparison of the optimization results for each objective, considering the limitations of the power transmission channel, is presented in Table 3. Based on an analysis of Figures 6 and 7, it is evident that, compared to Scenario 1, Scenario 2 achieves a significant increase in both the annual power generation and the minimum daily average power output. Specifically, the minimum daily average output, as constructed by Equation (1), increases by 73.08 MW, while the maximum daily average output decreases by 175.77 MW, resulting in a notable reduction in the peak-to-valley difference; the annual power generation, as constructed by Equation (2), increases by 1.3873 billion kWh, representing an enhancement of approximately 9.68%.

Table 3. Long-term optimization results.

Program	Minimum Output (MW)	Maximum Output (MW)	Power Generation (Billion kWh)
Scenario 1	480.01	3843	14.3310
Scenario 2	553.09	3667.23	15.7183

In summary, the long-term operation of the hydropower plant, targeting guaranteed output maximization (Equation (1)) and annual power generation (Equation (2)), significantly enhances both the power generation and power quality of the multi-energy complementary system. This improvement is reflected in a reduction in the peak-to-valley difference in output and an increase in power generation. Additionally, the optimized system reduces new energy power abandonment, although some abandonment still occurs during the abundant water period (August). However, while ensuring the benefits of the hydropower plant, the ability to smooth NE fluctuations through HWP multi-energy complementarity over the long term is primarily constrained by the annual regulation capacity of the reservoir. If the NE capacity becomes too large, the effectiveness of the long-term optimization may decline. An optimized HWP power output complementary diagram for Scenario 2 is displayed in Figure 8.

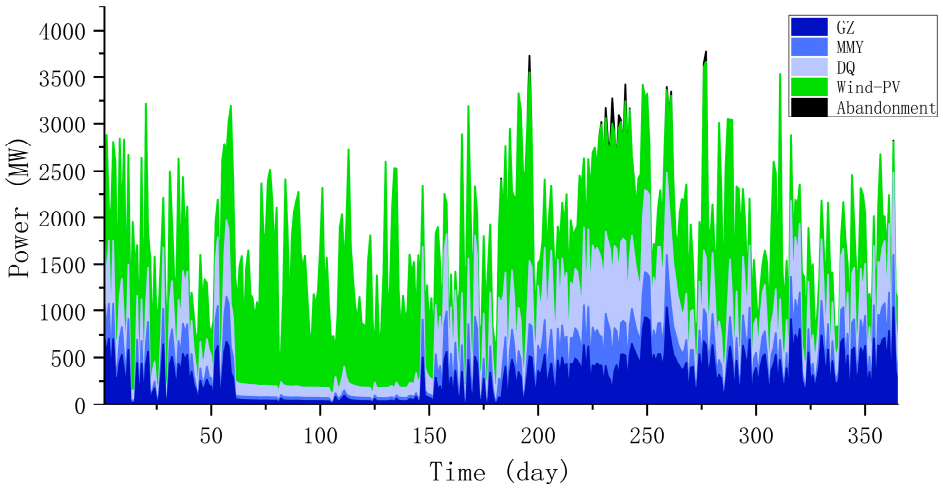


Figure 8. Complementary diagram of hydro–wind–PV power output.

5.2. Results of Short-Term Optimization for Hydro–Wind–PV System

5.2.1. Basic Parameters of Short-Term Optimization

(1) Based on the results from the long-term optimization, the short-term optimization results are analyzed using 3 January, 10 February, 25 April, 28 August, and 7 November as examples. The data for these five typical days are presented in Table 4.

Table 4. Initial and final reservoir capacity for each typical day.

Parameter	Date	GZ	MMY	DQ
Initial reservoir capacity (10^8 m^3)	3 January	20.81	1.365	8.82
	10 February	14.65	1.365	8.82
	25 April	10.5	1.365	8.82
	28 August	31.47	1.365	8.82
	7 November	30.35	1.365	8.82
Final reservoir capacity (10^8 m^3)	3 January	20.4	1.365	8.82
	10 February	14.43	1.365	8.82
	25 April	10.5	1.365	8.82
	28 August	31.88	1.365	8.82
	7 November	30.19	1.365	8.82

(2) Short-term optimization is based on MATLAB R2022a, calling upon the Yalmip toolbox, and solved using the Gurobi 11.0.3.

5.2.2. Results Analysis of Short-Term Optimization

In this study, two scenarios were constructed for comparative analysis to evaluate the effectiveness of the short-term optimization model:

(1) Scenario 1: Optimization of hydroelectricity alone.
(2) Scenario 2: Integrated optimization of hydro–wind–PV.

Energy complement plots for typical days under Scenario 1 and Scenario 2 are shown in Figures 9–13. The total generation, power abandonment, and residual load standard deviation for both scenarios are summarized in Table 5, where total generation represents the optimization results of Equation (13), power abandonment represents the optimization results of Equation (14), and residual load standard deviation represents the optimization results of Equation (15).

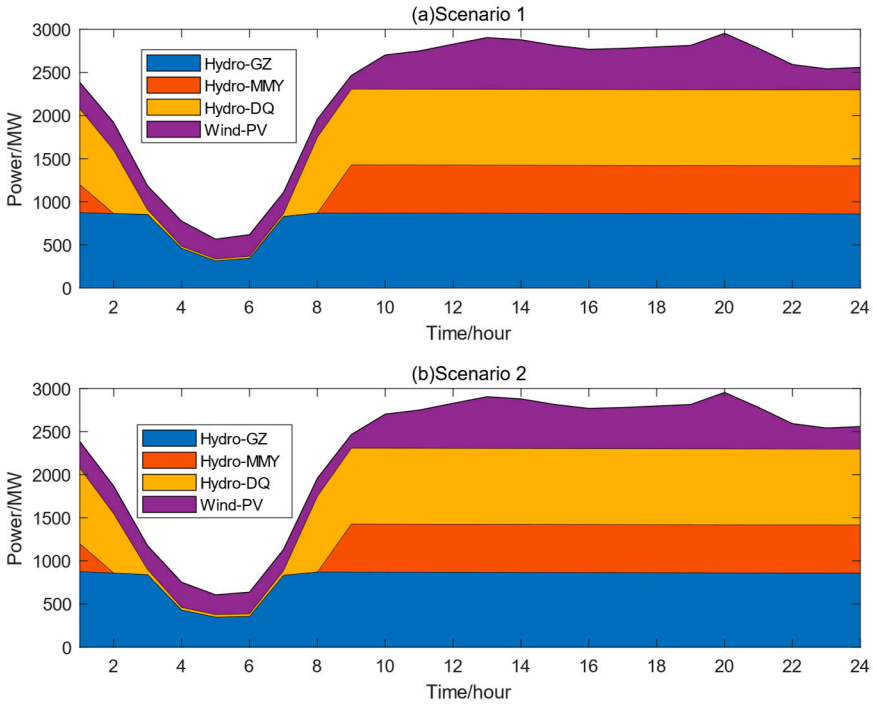


Figure 9. Short-term optimization comparison chart (3 January).

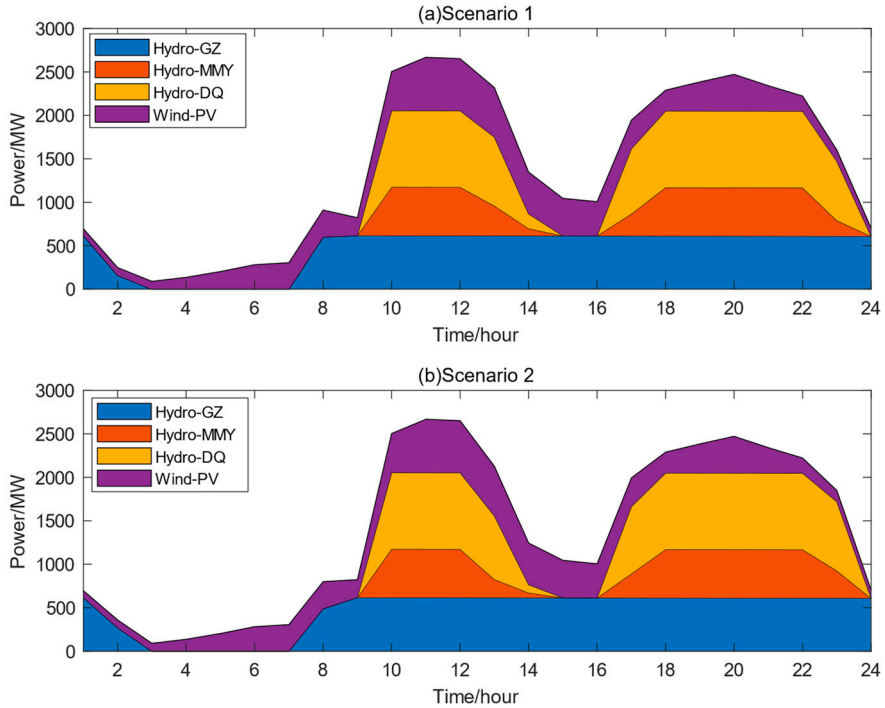


Figure 10. Short-term optimization comparison chart (10 February).

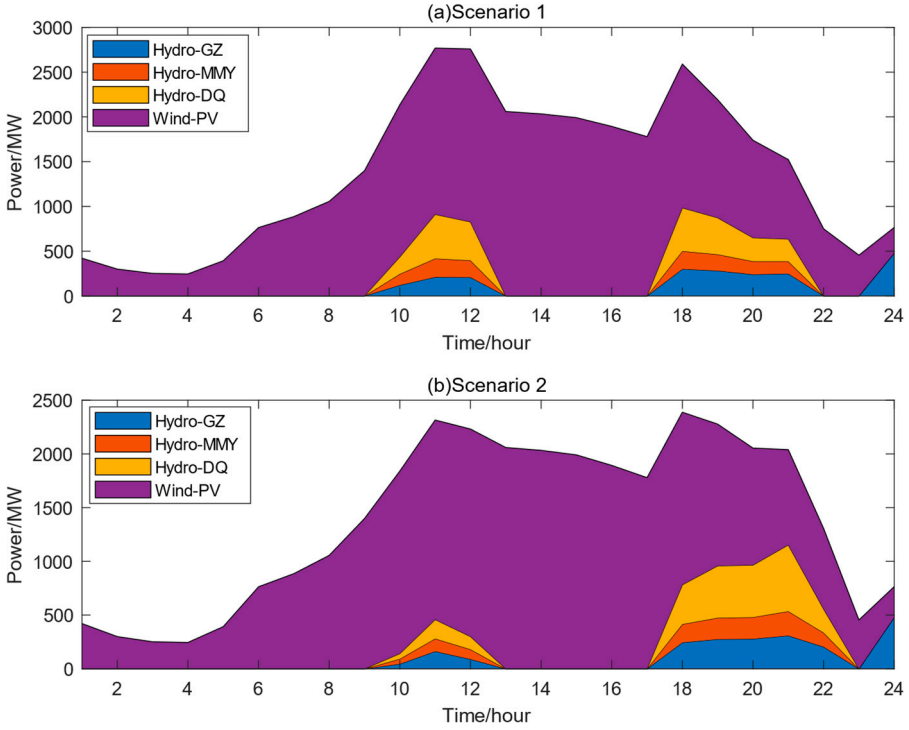


Figure 11. Short-term optimization comparison chart (25 April).

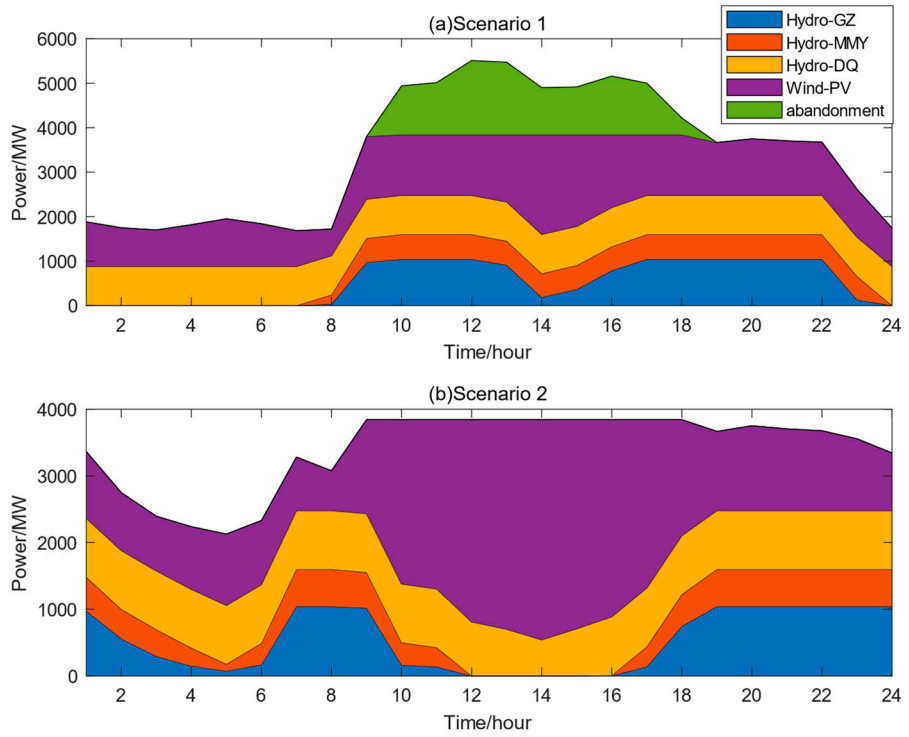


Figure 12. Short-term optimization comparison chart (28 August).

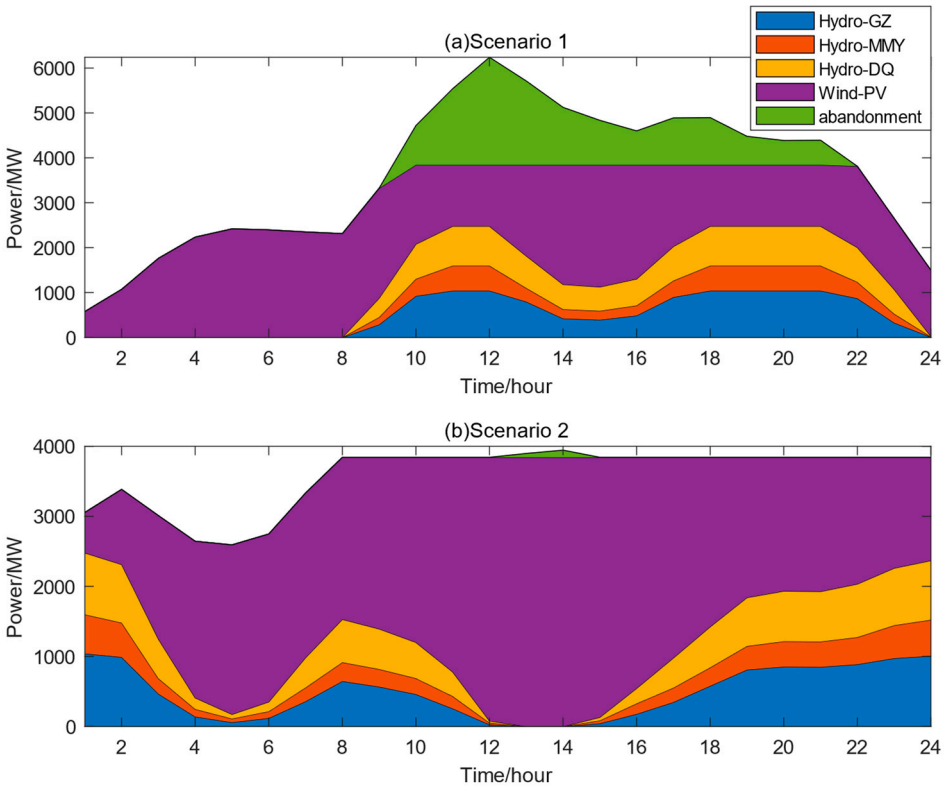


Figure 13. Short-term optimization comparison chart (7 November).

Table 5. Short-term optimization results.

Scenario	Date	Total Electricity (MWh)	Electricity Discarded (MWh)	Residual Load Standard Deviation (MW)
Scenario 1	3 January	54,448.24	0	2146.41
	10 February	33,202.33	0	2349.83
	25 April	33,148.22	0	2235.20
	28 August	71,892.36	10,559.00	1814.48
	7 November	72,544.47	13,718.01	1822.07
Scenario 2	3 January	54,448.18	0	2028.10
	10 February	33,202.33	0	1822.69
	25 April	33,148.22	0	1639.11
	28 August	81,689.54	0	1512.62
	7 November	86,105.68	156.80	1756.25

In analyzing Figures 9–13 and Table 5, it is evident that new energy generation on 3 January, 10 February, and 25 April is small. Under these conditions, the total power generation for Scenario 1 and Scenario 2 is the same. However, the standard deviations of the residual load for Scenario 2 are reduced by 118.31 MW, 527.14 MW, and 596.09 MW, respectively. On 28 August and 7 November, total power generation is higher, and Scenario 1 experiences significant power abandonment values of 10,559.00 MWh and 13,718.01 MWh, respectively. The standard deviation of the residual load is also larger at 1814.48 MW and 1822.07 MW. After optimization in Scenario 2, there is no power abandonment on 28 August, and only 156.80 MWh of power abandonment occurs on 7 November at around 14:00. At this time, as shown in Figure 13, hydroelectric output is reduced to zero, while NE output is very high, causing the new energy output to exceed the power transmission channel's limitations, which cannot be managed by hydropower alone. Additionally, the standard deviations of the residual load on 28 August and 7 November decrease by 301.86 MW and 65.82 MW, respectively.

In summary, while the hydroelectric power station's regulation capacity can smooth short-term fluctuations in new energy output, it struggles during periods of very high new energy generation. During these times, the output can exceed the power transmission channel's limits, leading to power abandonment, which hydropower alone cannot regulate. This indicates that the scale of HWP integration is primarily constrained by the hydroelectric power plant's regulation capacity and the limitations of the power transmission channel. When the installed capacity of NE is too large, additional measures, such as deploying energy storage batteries, are needed to assist the hydroelectric power plant in managing fluctuations.

5.3. Optimized Allocation of Ultra-Short-Term HESS

5.3.1. Basic Parameters of Ultra-Short-Term HESS

(1) This study focuses on the 5 min integrated output of wind power and photovoltaic energy at this HWP integration base. The total installed capacity of NE in the area is 5450 MW, comprising 2550 MW of wind power and 2900 MW of photovoltaic capacity. The basic parameter settings for the supercapacitor and battery energy storage systems are provided in Table 6.

Table 6. Basic parameters of supercapacitors and batteries.

Parameter	Supercapacitor	Battery
Unit capacity cost (CNY/kWh)	13,500	2700
Unit power cost (CNY/kW)	1500	640
O&M cost factor	0.05	0.05
Life of energy storage equipment (years)	25	15
Charge–discharge efficiency	0.95	0.9
SOC upper and lower limits	[0.1, 0.9]	[0.1, 0.9]
Discount rate (%)	5	5

(2) The HESS capacity configuration is based on MATLAB R2022a, calling upon the Yalmip toolbox, and solved using the Gurobi 11.0.3.

5.3.2. Results Analysis of Ultra-Short-Term HESS

(1) Typical Day Clustering Results

The K-means algorithm is applied to cluster NE data for the entire year, resulting in six wind power output scenarios. The number of days corresponding to each scenario is detailed in Table 7, and Figure 14 shows the 5 min new energy output curve of each typical day. In scenarios with extreme NE output data, the traditional K-means algorithm can cause distortion in the clustering centers. To address this, this paper uses the median of cumulative fluctuations as a criterion for selecting typical days. This involves calculating the cumulative fluctuations for all days within each scenario, ranking them, and selecting the median-ranked day as the typical day for that scenario. This approach to selecting typical days is less affected by extreme data, making it more reliable and convincing.

(2) Power decomposition results

Table 7. Frequency of each typical day.

Typical Day	Day1	Day2	Day3	Day4	Day5	Day6
Frequency (days)	88	49	21	121	61	25

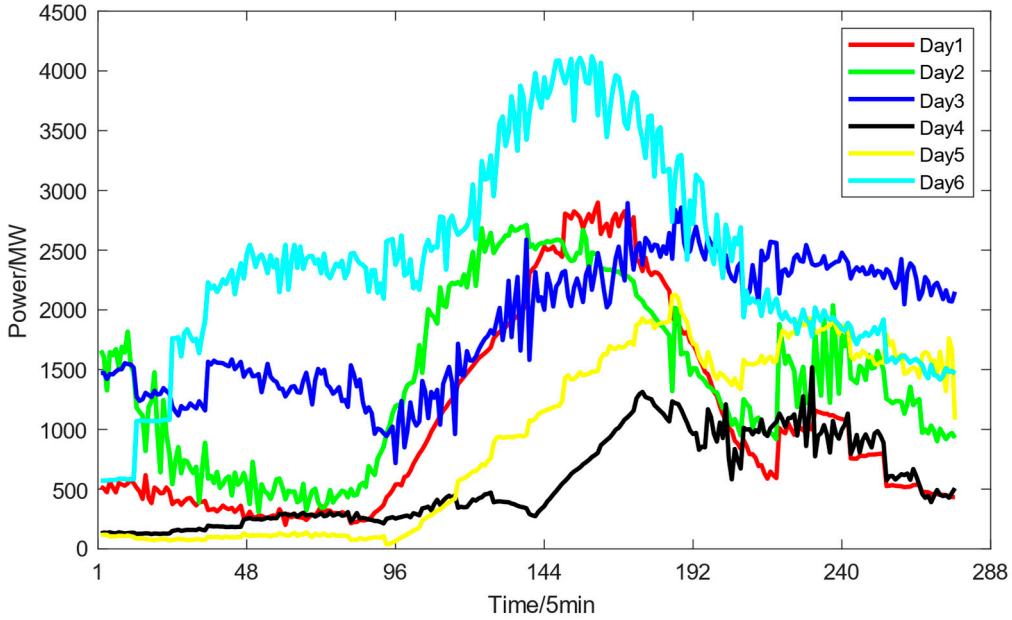


Figure 14. Typical day new energy output.

In this paper, the PSO, WOA, NGO, RIME, and CPO are employed to optimize the parameters of ICEEMDAN. Power decomposition is then performed for a typical day. A comparison of the performance of each algorithm is illustrated in Figure 15. The figure demonstrates that using CPO yields superior decomposition results compared to the other algorithms.

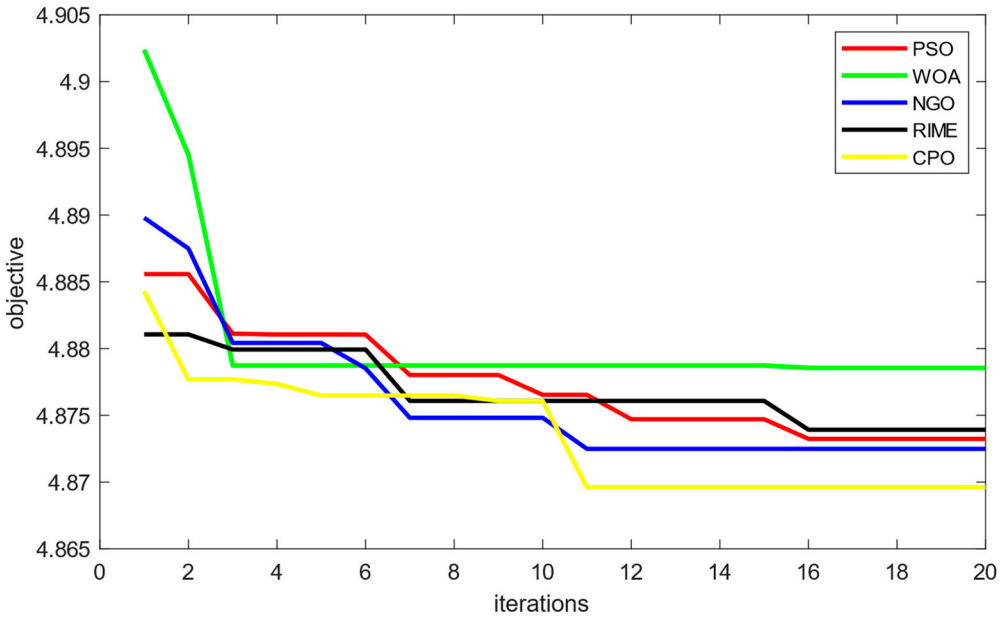


Figure 15. Comparison of different algorithms to optimize ICEEMDAN parameters.

The direct grid-connected power and energy storage power tasks are determined using a grid-connected fluctuation limit of 125 MW as the threshold. Figure 16 displays the maximum fluctuation amount for each order component following low-frequency reconfigurations for each typical day. Components exceeding 125 MW are allocated to energy storage power tasks, while those below 125 MW are assigned as direct grid-connected power. This approach keeps the fluctuation within a small range. The direct grid-connected

power and storage smoothing components for the typical period are derived after sequentially connecting six typical days, as illustrated in Figure 17.

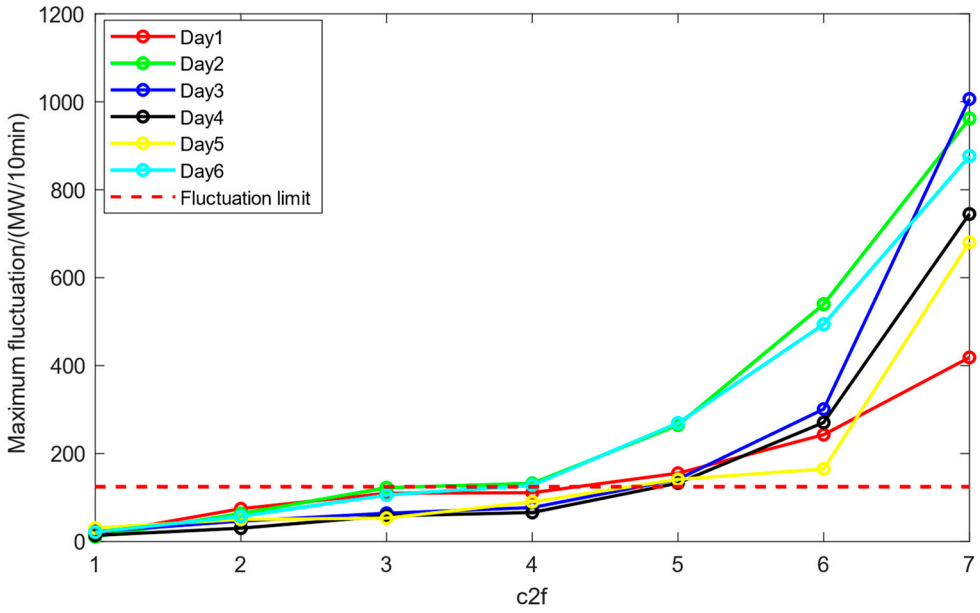


Figure 16. Maximum fluctuation of low-frequency reconstruction components of each order.

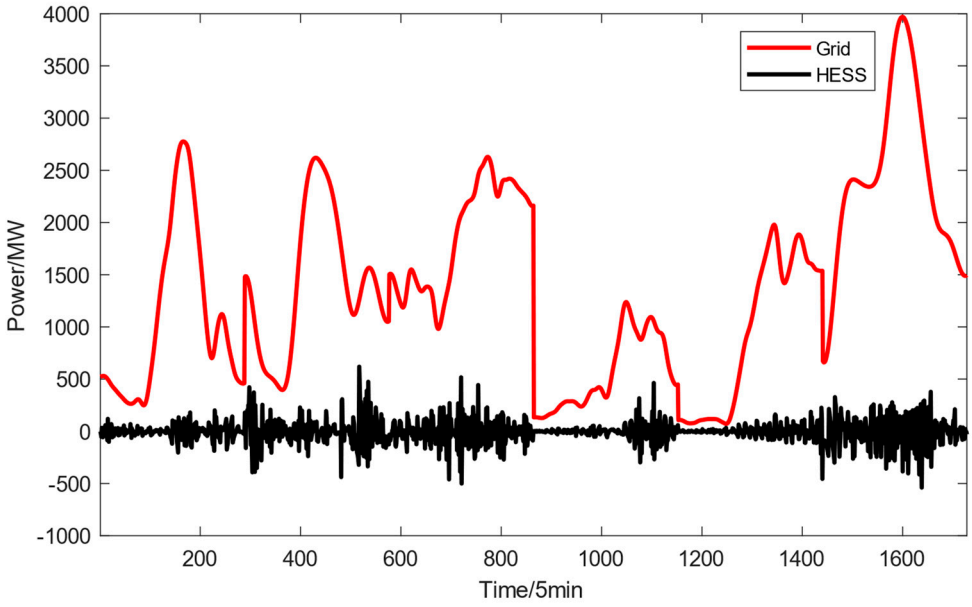


Figure 17. Direct grid-connected power and storage smoothing power.

(3) Analysis of HESS configuration results

Four scenarios are established for comparison, based on the curves in Figure 18, which illustrate the change in investment and volatility as a function of the multiplier of the volatility penalty cost.

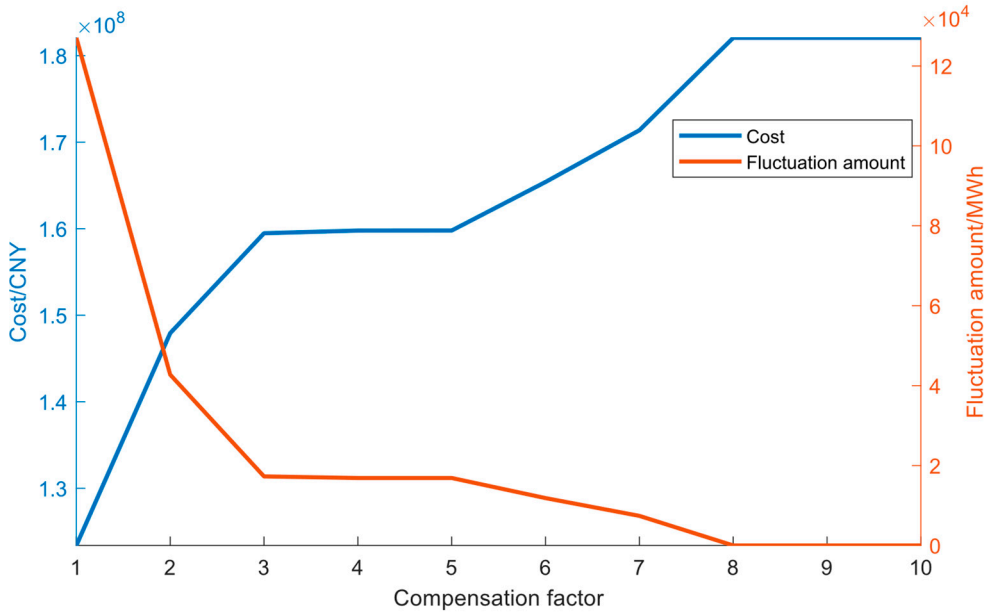


Figure 18. Changes in investment and fluctuation volumes.

Scenario 1: Zero baseline; fluctuation compensation cost multiplier set to 8;
Scenario 2: Variable baseline; fluctuation compensation cost multiplier set to 1;
Scenario 3: Variable baseline; fluctuation compensation cost multiplier set to 8;
Scenario 4: Variable baseline using only supercapacitors.

The results of the HESS configuration for the three scenarios are shown in Table 8.

Table 8. HESS configuration results.

Parameter	Scenario 1	Scenario 2	Scenario 3	Scenario 4
Supercapacitor cost (CNY)	99,460,281.32	71,338,122.90	71,081,685.30	443,202,641.67
Battery cost (CNY)	38,645,708.84	51,081,190.90	118,327,610.09	-
Consolidated cost (CNY)	138,105,990.16	122,419,313.80	189,409,295.39	443,202,641.67
Fluctuation (MWh)	482,066.34	127,039.07	0.00	0.00
Baseline (MW)	0.00	−6.88	−16.85	−15.24
Supercapacitor capacity (MWh)	64.55	51.31	51.09	387.66
Supercapacitor power (MW)	311.08	210.26	223.32	634.18
Battery capacity (MWh)	114.79	177.23	398.62	-
Battery power (MW)	307.86	238.59	412.47	-

The effects of smoothing fluctuations for Scenarios 1, 2, 3, and 4 are presented in Figure 19. In Figure 19a, using 0 MW as the baseline, the positive fluctuation components are mostly absorbed and compensated due to the limitations of charging and discharging efficiency. However, more negative fluctuation components remain unabsorbed, resulting in a total fluctuation of 482,066.34 MWh. Figure 19b reveals that, with a variable baseline, the total cost for the HESS in Scenario 2 is lower than in Scenario 1. Most fluctuation components are absorbed and compensated, although some larger amplitude points are not fully compensated, reducing the total fluctuation to 127,039.07 MWh. In Figure 19c, Scenario 3 employs larger fluctuation compensation cost coefficients, leading to a higher total cost than Scenarios 1 and 2. Nonetheless, all fluctuation components are absorbed and compensated, and the baseline shifts downward to −16.85 MW. Scenario 4 uses only supercapacitors to realize the full compensation of fluctuating volume, and the combined cost of this scenario is about 2.49 times that of Scenario 3, which is much less economical than the previous three scenarios. These findings suggest that using a variable baseline can achieve better smoothing results at a lower cost. Increasing the fluctuation compensation cost coefficient allows for the full compensation of fluctuations.

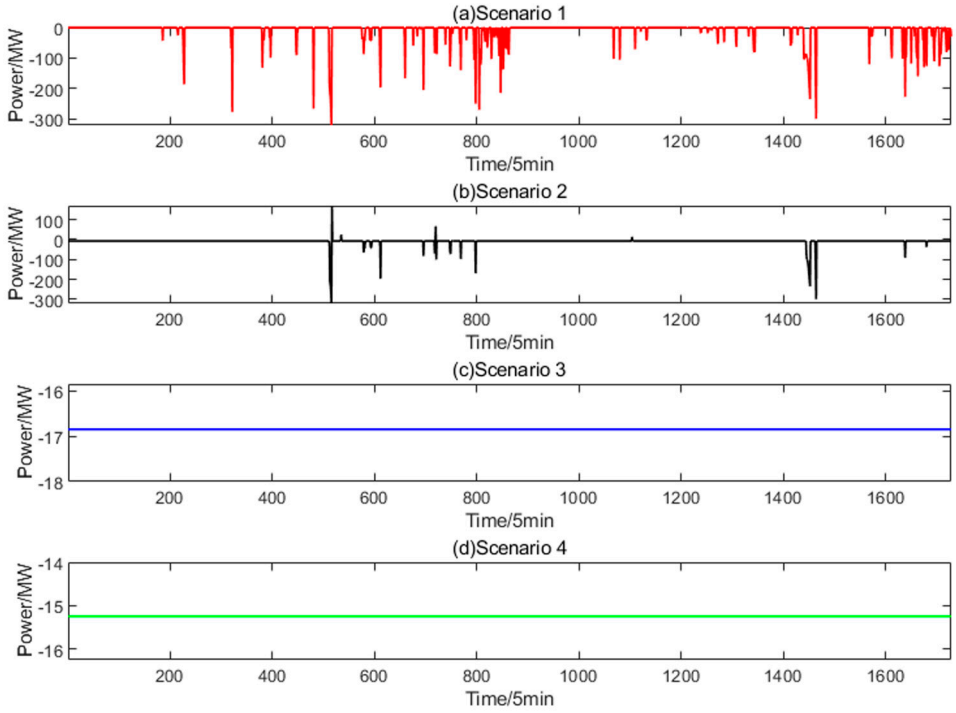


Figure 19. Comparison of fluctuations after optimization.

Figure 20 shows grid-connected power curves for Scenario 1, Scenario 2, and Scenario 3 after configuring the HESS. In comparison, Scenario 3 demonstrates a significantly better fluctuation smoothing effect than Scenario 1 and Scenario 2, fully validating the effectiveness of the established HESS model in mitigating wind power fluctuations. Considering both the cost and the level of fluctuation, this paper selects Scenario 3 to fully compensate for the fluctuations.

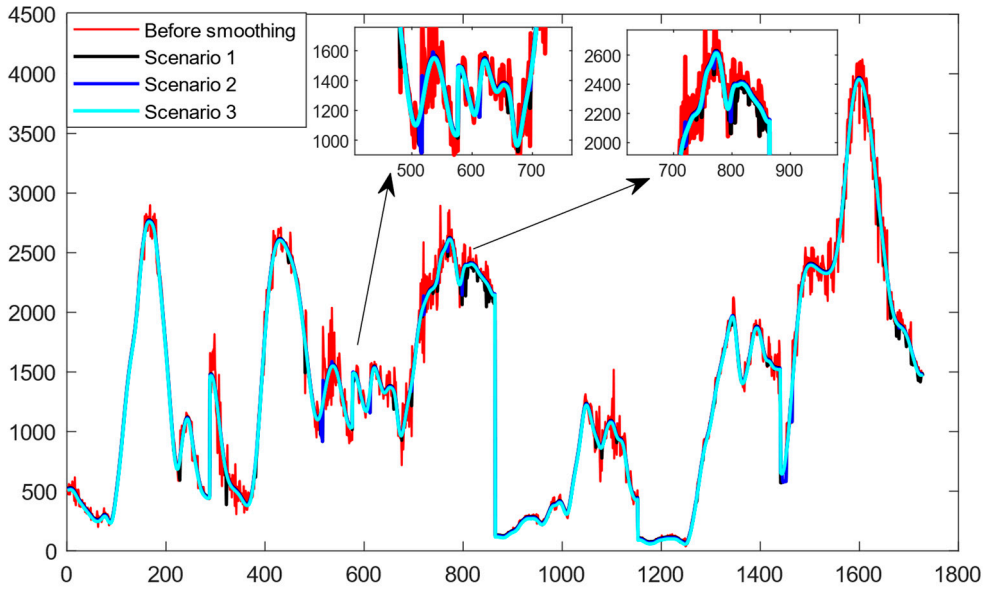


Figure 20. Optimized grid-connected power of NE.

Figure 21 illustrates the operating conditions of the HESS in Scenario 3 proposed in this paper. From Figure 21a, we can see that, due to the small capacity of the supercapacitor, it frequently operates at a high depth of charge and discharge, resulting in a high percentage of operating time. Meanwhile, the SOC curve in Figure 21b shows that, due to the large

capacity of the electrochemical energy storage, it mainly operates in "shallow charging and shallow discharging" mode. This is beneficial for prolonging its service life. The SOC mostly remains between 0.3 and 0.5, providing sufficient power and capacity to smooth fluctuations.

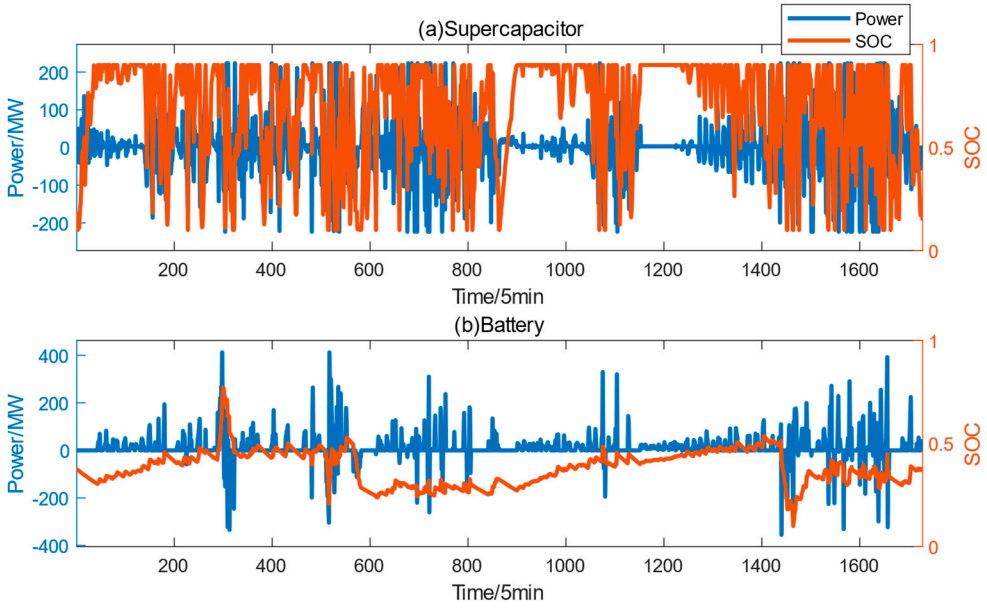


Figure 21. Charge–discharge power and SOC of Scenario 3.

In summary, the ability of the HESS to smooth ultra-short-term NE fluctuations is primarily influenced by its capacity. By adjusting the penalty multiplier for fluctuation amplitude in the cost function, the model can effectively smooth fluctuations. Furthermore, the role of the HESS can be better utilized by lowering the baseline of the fluctuation amplitude to be smoothed, thereby reducing the overall cost. However, due to the high cost of a single supercapacitor unit, relying solely on supercapacitors to smooth ultra-short-term fluctuations proves to be expensive. Until the price of supercapacitors decreases, adopting a HESS offers certain advantages.

6. Conclusions

In this paper, a model for optimizing the operation of HWP integration and allocating ultra-short-term energy storage capacity is proposed. The following conclusions are drawn from a simulation study conducted on the Beipanjiang HWP complementary project in China:

(1) After conducting the long-term simulation, the annual power generation increased by 1.3873 billion kWh, representing an improvement of approximately 9.68%. The minimum daily average output increased by 73.08 MW, while the maximum daily average output decreased by 175.77 MW, leading to a significant reduction in the peak-to-valley difference.

(2) By utilizing the hydropower station's regulating capacity, the complementarity of a hydro-wind-PV system can be achieved on a short-term timescale, significantly reducing both the standard deviation of the residual load and the amount of power abandonment. However, during periods of very high new energy power generation, when the station's output exceeds the limits of the power transmission channel, hydropower alone cannot fully regulate these fluctuations, resulting in some power being abandoned. Nonetheless, the amount of power abandonment is reduced compared to pre-optimization levels.

(3) To smooth ultra-short-term fluctuations in new energy output, a lithium-ion battery energy storage system with a capacity of 398.62 MW and power of 412.47 MW and a supercapacitor energy storage system with a capacity of 51.09 MW and power of 223.32 MW are configured. Additionally, analysis shows that using a variable baseline can provide more

effective fluctuation compensation at a lower cost. Complete compensation for fluctuations can be achieved by adjusting the fluctuation compensation cost coefficient.

The current study remains focused on the power plant level, primarily achieving the long-term and short-term operation optimization of HWP integration by adjusting the overall output of a hydropower plant. Ultra-short-term fluctuations in new energy sources are smoothed through the configuration of the HESS. However, the adjustment of hydropower plant output does not account for in-plant operational variables, such as unit and gate operations. Additionally, the configuration of the HESS considers only capacity and power allocation, without addressing the spatial distribution of energy storage plants or the internal operation strategies of the HESS. In the future, an integrated scheduling and operation mechanism, along with models and rules, will be developed for more detailed spatial classification across "power station groups, individual power stations, and in-plant operations".

Author Contributions: Conceptualization, H.W.; methodology, H.W. and C.F.; software, C.F.; validation, H.W. and C.F.; formal analysis, J.Z. and H.W.; investigation, C.F.; resources, H.W. and C.F.; data curation, C.F.; writing—original draft preparation, C.F.; writing—review and editing, H.W., J.Z., J.H. and X.Z.; visualization, C.F.; supervision, H.W., J.Z., J.H. and X.Z.; project administration, J.Z. and H.W.; funding acquisition, J.Z. All authors have read and agreed to the published version of the manuscript.

Funding: This work is supported in part by the National Key Research and Development Program Project (grant number: 2019YFE0104800), the Scientific and Technological Innovation Team of Colleges and Universities in Henan Province (grant number: 22IRTSTHN011), and the Scientific and Technological Research Project of Henan Provincial Department of Education (grant number: 20A210027).

Data Availability Statement: The data are contained within the article.

Conflicts of Interest: The authors declare no conflicts of interest.

Abbreviations

BESS	battery energy storage system
CEEMDAN	Complete Ensemble Empirical Mode Decomposition with Adaptive Noise
CHBMC	cascaded H-bridge multilevel converter
CPO	Crested Porcupine Optimizer
DBO	Dung Beetle Optimizer
DE	Differential Evolution
ESS	energy storage system
EEMD	Ensemble Empirical Mode Decomposition
FTC	fault-tolerant control
HESS	Hybrid Energy Storage System
HWP	hydro–wind–photovoltaic
HRESs	hybrid renewable energy systems
ICEEMDAN	Improved Complete Ensemble Empirical Mode Decomposition with Adaptive Noise
MECB	multi-energy complementary base
MILP	mixed-integer linear programming
NE	new energy
NGO	Northern Goshawk Optimization
OC	open-circuit
PSO	Particle Swarm Optimization
PV	photovoltaic
THD	total harmonic distortion
TTAO	Triangulation Topology Aggregation Optimizer
RIME	Rime optimization algorithm
SOC	state of charge
UHV	ultra-high voltage
WOA	Whale Optimization Algorithm

References

1. Zhang, H.; Lu, Z.; Hu, W.; Wang, Y.; Dong, L.; Zhang, J.; Zhang, H.; Lu, Z.; Hu, W.; Wang, Y.; et al. Coordinated optimal operation of hydro–wind–solar integrated systems. *Appl. Energy* **2019**, *242*, 883–896. [CrossRef]
2. Abera, F.; Asfaw, D.; Engida, A.; Melesse, A. Optimal Operation of Hydropower Reservoirs under Climate Change: The Case of Tekeze Reservoir, Eastern Nile. *Water* **2018**, *10*, 273. [CrossRef]
3. Xu, J.; Wang, F.; Lv, C.; Xie, H. Carbon emission reduction and reliable power supply equilibrium based daily scheduling towards hydro-thermal-wind generation system: A perspective from China. *Energy Convers. Manag.* **2018**, *164*, 1–14. [CrossRef]
4. An, Y.; Fang, W.; Ming, B.; Huang, Q. Theories and methodology of complementary hydro/photovoltaic operation: Applications to short-term scheduling. *J. Renew. Sustain. Energy* **2015**, *7*, 063133. [CrossRef]
5. Kougias, I.; Szabó, S.; Monforti-Ferrario, F.; Huld, T.; Bódis, K. A methodology for optimization of the complementarity between small-hydropower plants and solar PV systems. *Renew. Energy* **2016**, *87*, 1023–1030. [CrossRef]
6. Zhu, F.; Zhong, P.-A.; Sun, Y.; Xu, B.; Ma, Y.; Liu, W.; Zhang, D.; Dawa, J. A coordinated optimization framework for long-term complementary operation of a large-scale hydro-photovoltaic hybrid system: Nonlinear modeling, multi-objective optimization and robust decision-making. *Energy Convers. Manag.* **2020**, *226*, 113543. [CrossRef]
7. Yuan, W.; Liu, Z.; Su, C.; Wang, X. Photovoltaic capacity optimization of small and medium-sized hydro-photovoltaic hybrid energy systems considering multiple uncertainties. *J. Clean. Prod.* **2020**, *276*, 124170. [CrossRef]
8. Yang, Y.; Zhou, J.; Liu, G.; Mo, L.; Wang, Y.; Jia, B.; He, F. Multi-plan formulation of hydropower generation considering uncertainty of wind power. *Appl. Energy* **2020**, *260*, 114239. [CrossRef]
9. Wang, L.; Ma, S.; Wang, H.; Zhou, Q.; Hu, J.; Wu, F.; Ye, C. Multi-objective Capacity Configuration for Wind and Photovoltaic Power Generation Considering Retrofitting Cascade Hydropower with Pumped Storage. *Water Power* **2024**, *50*, 1–8.
10. Wen, X.; Liu, F.; Tan, Q.; Wang, H. Research on short-term multi-level and multi-objective optimal scheduling of cascade hydropower stations under complex water resources and power constraints. *Shuili Xuebao/J. Hydraul. Eng.* **2023**, *54*, 392–404.
11. Ma, C.; Liu, L. Optimal capacity configuration of hydro-wind-PV hybrid system and its coordinative operation rules considering the UHV transmission and reservoir operation requirements. *Renew. Energy* **2022**, *198*, 637–653. [CrossRef]
12. Apostolopoulou, D.; Mcculloch, M. Optimal Short-Term Operation of a Cascaded Hydro-Solar Hybrid System: A Case Study in Kenya. *IEEE Trans. Sustain. Energy* **2019**, *10*, 1878–1889. [CrossRef]
13. Tan, Q.; Wen, X.; Sun, Y.; Lei, X.; Wang, Z.; Qin, G. Evaluation of the risk and benefit of the complementary operation of the large wind-photovoltaic-hydropower system considering forecast uncertainty. *Appl. Energy* **2021**, *285*, 116442. [CrossRef]
14. Liu, W.; Zhu, F.; Chen, J.; Wang, H.; Xu, B.; Song, P.; Zhong, P.-A.; Lei, X.; Wang, C.; Yan, M.; et al. Multi-objective optimization scheduling of wind–photovoltaic–hydropower systems considering riverine ecosystem. *Energy Convers. Manag.* **2019**, *196*, 32–43. [CrossRef]
15. He, Y.; Hong, X.; Wang, C.; Qin, H. Optimal capacity configuration of the hydro-wind-photovoltaic complementary system considering cascade reservoir connection. *Appl. Energy* **2023**, *352*, 121927. [CrossRef]
16. Ren, Y.; Yao, X.; Liu, D.; Qiao, R.; Zhang, L.; Zhang, K.; Jin, K.; Li, H.; Ran, Y.; Li, F. Optimal design of hydro-wind-PV multi-energy complementary systems considering smooth power output. *Sustain. Energy Technol. Assess.* **2022**, *50*, 101832. [CrossRef]
17. Ming, B.; Liu, P.; Cheng, L.; Zhou, Y.; Wang, X. Optimal daily generation scheduling of large hydro–photovoltaic hybrid power plants. *Energy Convers. Manag.* **2018**, *171*, 528–540. [CrossRef]
18. Zhang, Y.; Lian, J.; Ma, C.; Yang, Y.; Pang, X.; Wang, L. Optimal sizing of the grid-connected hybrid system integrating hydropower, photovoltaic, and wind considering cascade reservoir connection and photovoltaic-wind complementarity. *J. Clean. Prod.* **2020**, *274*, 123100. [CrossRef]
19. Lu, L.; Yuan, W.; Su, C.; Wang, P.; Cheng, C.; Yan, D.; Wu, Z. Optimization model for the short-term joint operation of a grid-connected wind-photovoltaic-hydro hybrid energy system with cascade hydropower plants. *Energy Convers. Manag.* **2021**, *236*, 114055. [CrossRef]
20. Zhang, Y.; Ma, C.; Yang, Y.; Pang, X.; Liu, L.; Lian, J. Study on short-term optimal operation of cascade hydro-photovoltaic hybrid systems. *Appl. Energy* **2021**, *291*, 116828. [CrossRef]
21. Tan, Q.; Zhang, Z.; Wen, X.; Fang, G.; Xu, S.; Nie, Z.; Wang, Y. Risk control of hydropower-photovoltaic multi-energy complementary scheduling based on energy storage allocation. *Appl. Energy* **2024**, *358*, 122610. [CrossRef]
22. Gao, X.; Wang, L.; Sun, H.; Tian, J.; Wang, Z.; Jiang, J.; Guo, W. Research on optimal configuration of hybrid energy storage system based on improved CEEMDAN. *Energy Rep.* **2021**, *7*, 1308–1318. [CrossRef]
23. Zhang, J.; Zhang, T.; Cheng, P.; Yang, D.; Yan, J.; Tian, X. Optimal Allocation of Hybrid Energy Storage System Based on Smoothing Wind Power Fluctuation and Improved Scenario Clustering Algorithm. *Processes* **2023**, *11*, 3407. [CrossRef]
24. Xie, D.; Lin, C.; Deng, Q.; Lin, H.; Cai, C.; Basler, T.; Ge, X. Simple Vector Calculation and Constraint-Based Fault-Tolerant Control for a Single-Phase CHBMC. *IEEE Trans. Power Electron.* **2024**, *40*, 2028–2041. [CrossRef]
25. Yu, X.; Li, G.; Li, Y.; Wang, B.; Cheng, C. Short-term Robust Optimization Scheduling of Cascade Hydropower Stations Coupled With Daily Contract Decomposition and Day-ahead Market Bidding. *Dianwang Jishu/Power Syst. Technol.* **2021**, *45*, 4016–4024.
26. Zhao, S.; Zhang, T.; Cai, L.; Yang, R. Triangulation topology aggregation optimizer: A novel mathematics-based meta-heuristic algorithm for continuous optimization and engineering applications. *Expert Syst. Appl.* **2024**, *238*, 121744. [CrossRef]
27. Xue, J.; Shen, B. Dung beetle optimizer: A new meta-heuristic algorithm for global optimization. *J. Supercomput.* **2022**, *79*, 7305–7336. [CrossRef]

28. Su, H.; Zhao, D.; Heidari, A.A.; Liu, L.; Zhang, X.; Mafarja, M.; Chen, H. RIME: A physics-based optimization. *Neurocomputing* **2023**, *532*, 183–214. [CrossRef]
29. Colominas, M.A.; Schlotthauer, G.; Torres, M.E. Improved complete ensemble EMD: A suitable tool for biomedical signal processing. *Biomed. Signal Process. Control* **2014**, *14*, 19–29. [CrossRef]
30. Abdel-Basset, M.; Mohamed, R.; Abouhawwash, M. Crested Porcupine Optimizer: A new nature-inspired metaheuristic. *Knowl. Based Syst.* **2024**, *284*, 111257. [CrossRef]
31. Mirjalili, S.; Lewis, A. The Whale Optimization Algorithm. *Adv. Eng. Softw.* **2016**, *95*, 51–67. [CrossRef]
32. Dehghani, M.; Hubalovsky, S.; Trojovsky, P. Northern Goshawk Optimization: A New Swarm-Based Algorithm for Solving Optimization Problems. *IEEE Access* **2021**, *9*, 162059–162080. [CrossRef]

Disclaimer/Publisher's Note: The statements, opinions and data contained in all publications are solely those of the individual author(s) and contributor(s) and not of MDPI and/or the editor(s). MDPI and/or the editor(s) disclaim responsibility for any injury to people or property resulting from any ideas, methods, instructions or products referred to in the content.